ELSEVIER

Deep-Sea Research II 51 (2004) 2943–2971

DEEP-SEA RESEARCH
PART II

www.elsevier.com/locate/dsr2

Near-bed solibores over the continental slope in the Faeroe-Shetland Channel

Phil Hosegood*, Hans van Haren

Royal Netherlands Institute of Sea Research (NIOZ), P.O. Box 59, 1790 AB Den Burg, The Netherlands

Abstract

On two occasions within a 12-day measurement period in the Faeroe-Shetland Channel, strongly nonlinear wave trains were observed at the sea-bed, propagating *up* the continental slope in water depths >450 m. The events were separated by a period of 4 days and, whilst resembling in appearance a density current running up a slope, are termed 'solibores', displaying the properties of both turbulent internal bores and nonlinear internal solitary waves (ISW). Each solibore displays a steep leading edge followed by a train of nonlinear waves with amplitudes of $O(10\,\mathrm{m})$ and periods of $\sim$5–20 min. Wave-induced particle velocities are consistent with ISW, whilst a zone of strong horizontal convergence at the leading edge of the solibores causes the formation of a rotor with flow in the opposite sense to a 'forward overturning' surface wave. In both cases upward vertical velocities $>10\,\mathrm{cm\,s^{-1}}$ are immediately followed by a return downward flow of equal magnitude. A CTD and microstructure transect conducted during the passage of the first solibore illustrates its behaviour as an up-slope intrusion of cold, dense water with concurrent rates of turbulent dissipation, ε, of $O(10^{-7}\,\mathrm{W\,kg^{-1}})$ and resulting in short-term maximum vertical diffusivities, K_z, of $O(10^{-1}\,\mathrm{m^2\,s^{-1}})$. In the long-term however, $K_z<10^{-4}\,\mathrm{m^2\,s^{-1}}$, implying that the solibores are not important for sustaining deep-sea mixing. In contrast, sediment fluxes at 2 and 30 m above the bed during the first solibore are $O(10^2)$ larger than the background value, implying solibores are the dominant sediment transport mechanism despite their intermittent occurrence. The transport of sediment, up the slope in the direction of propagation of the solibore, is contrary to the usually considered pathway for sediment from coastal seas to the abyss via the continental slope. That sediment transport is dominated by short-term events appears to be corroborated by long-term data (>140 days) which again indicate intermittency in periods of enhanced sediment flux. The solibores are consistent with the results of numerical and laboratory experiments on hydraulic jumps resulting from shoaling ISW. The influence of the slope is proposed to be the reason for their slightly different forms and effects on sediment transport; thus the first solibore, propagating directly up the slope, is proposed to result from an overturning hydraulic jump caused by kinematic instabilities and which subsequently forms a horizontal density intrusion. The second solibore represents a dispersive wave train due its oblique direction of propagation which reduces the effective bottom-slope, allowing dispersion to balance nonlinear effects and prohibiting overturning.

*Corresponding author. Tel.: +31 222 369406; fax: +31 222 319674.
E-mail address: hosegood@nioz.nl (P. Hosegood).

0967-0645/$ - see front matter © 2004 Elsevier Ltd. All rights reserved.
doi:10.1016/j.dsr2.2004.09.016

1. Introduction

The continental slope strongly influences the hydrodynamics in its vicinity and has consequences for mixing processes and the transport of sediments and nutrients. The interaction of internal waves, especially their critical reflection (Eriksen, 1982), with the slope has traditionally been proposed to account for the enhanced mixing required to maintain the meridional overturning circulation (Munk, 1966; Munk and Wunsch, 1998), whilst internal tides promote mixing both at the slope where they are generated and reflected (New and Pingree, 1990), and in the ocean interior where they may propagate as distinct beams of energy (for example, Pingree et al., 1986) or interfacial waves propagating along the pycnocline (Holloway, 1987; Small et al., 1999). The latter case in particular is often observed in shelf seas as the degeneration of an internal tidal wave into an internal bore or a packet of solitons. In response to observations of such internal waves, Henyey and Hoering (1997) coined the term 'solibore' to define the high frequency internal waves which display the properties of turbulent internal bores whilst being accompanied by short-period intense pulse-like internal waves which display the characteristics of solitons or internal solitary waves (ISWs). The ISWs are of permanent form with a 'sech^2' profile, extending into the thicker of the two layers between which they propagate, with the consequence that they are usually observed as waves of depression given the location of the near surface thermocline. Internal bores and hydraulic jumps typically result from the nonlinear steepening of, in the ocean, an internal tidal wave or, in lakes, of a wind-forced basin-scale wave. They exhibit strong dissipation and shear, with the linear long wave phase speed behind the bore exceeding the speed of the bore itself (Henyey and Hoering, 1997).

The ambiguity in observations that prompted the definition of a solibore can arise due to the time at which observations are made. A solibore begins like a bore in which nonlinear steepening dominates, before becoming more wavelike as the energy supply is reduced and with it the amplitude and dissipation of the bore, with dispersion subsequently balancing the nonlinearity as in a train of solitons. Thus whether a solibore appears in observations more as a bore or a nonlinear wave train may be simply a consequence of at what stage of its evolution the measurements are made. Observations from shelf breaks (Holloway, 1987; Small et al., 1999; Colosi et al., 2001; Johnson et al., 2001) indicate the manifestation of the shoreward propagating internal tide as an internal bore. In each case, however, the bore is accompanied by, or evolves into, packets of solitary waves. Observations on the continental shelf proper suggest the form of the internal tidal wave to be a packet of nonlinear waves, or more specifically solitons (Sandstrom and Elliot, 1984; Howell and Brown, 1985; Jeans and Sherwin, 2001a, b) consistent with the concept of the solibore beginning more as a bore before evolving into a wave train. Solibores with vertical displacements in excess of 100 m are also common due to tidal forcing in the Straits of Gibraltar (Wesson and Gregg, 1988; Morozov et al., 2002) and are typically accompanied by short-period internal waves which have been described as solitons (Bryden et al., 1994).

Whilst a solibore was originally defined to describe the evolution of internal tides, the term may be extended to include features that demonstrate the same bore-like properties accompanied by high-frequency solitary waves but which are forced by motions other than the tide. Solibores may be forced by the wind in lakes where internal seiches and standing waves steepen during their propagation along the axis of the lake (Hunkins and Fliegel, 1973; Thorpe, 1977; Horn et al., 2001). Horn et al. (2001) found the evolution of a wind induced, interfacial gravity wave into either a train of solitons or a turbulent internal bore, accompanied by strong dissipation and mixing due to localised shear-induced turbulence, to be dependent on the initial amplitude of the wave. A larger initial wave tended towards the formation of a bore. ISWs observed near a steepened Kelvin wave front and at the head of an intrusive thermocline jet in Lake Biwa and Lake Kinneret potentially contain as much as 1% of the basin-scale Kelvin wave energy and represent an important pathway for the transferral of large-scale energy to small scales which are available for mixing as the ISWs shoal at the lake perimeter (Boegman et al., 2003).

Shoaling ISWs have been shown recently in numerical and laboratory experiments to result in solibore-like features. Vlasenko and Hutter (2002) study numerically the shoaling of intense ISWs of depression propagating from deep water onto the shelf. When conditions are conducive for breaking, nonlinearity causes the rear face of the ISW to steepen, forming a baroclinic bore, which eventually overturns due to kinematic instabilities to produce 'soliton-like waves of elevation'. Such waves were also observed by Wallace and Wilkinson (1988), Helfrich (1992) and Lamb (2002) and are also referred to as 'turbulent boluses' and 'solitary-like waves with trapped cores'. They are however not positive solitary waves but rather exhibit similar behaviour; they correspond qualitatively to the crests on a wave packet that would be caused by the topographic scattering of a solitary wave of depression incident on a slope-shelf topography into a dispersive wave packet with waves of elevation (Djordjevic and Redekopp, 1978; Helfrich et al., 1984). The scattering process is interrupted when the interface intersects the slope with the boluses forming rather than a wave packet. The overturned wave then behaves as an upstream propagating pulsating jet, which exhibits wave-like undulations on its upper edge and whose crests extend into the thicker overlying layer. In contrast, Lamb (2002) proposes that the waves which form the wave packet resulting from a breaking ISW are indeed consistent with genuine ISWs rather than turbulent boluses, with the eventual wave field composed of a large leading solitary wave followed by one or two smaller solitary waves and then a mode-one wave train, a mode-two wave and other higher-mode waves. In some respects the pulsating jet may resemble a density current propagating up a slope, with the dense fluid penetrating beneath the lighter fluid higher on the slope. Such currents have been observed in the laboratory, where the initial head is cut off from the dense flow resulting in the formation of a new head behind it due to the interaction between the current and waves set up by its advancement (Simpson, 1997). Under no circumstances however has such a current been observed to generate a nonlinear dispersive train, whereas for less steep slopes than that required for the overturning of an ISW, dispersion has time to balance nonlinearity and permit the development of a dispersive wave tail behind the steep bore-like leading face. Thus despite an apparently different forcing mechanism it appears that a shoaling ISW, or indeed a travelling hydraulic jump at the seabed, may display the properties of a solibore. We thus extend the use of the term throughout this paper to refer to near-bed features that exhibit bore-like features in conjunction with short-period internal waves.

In this paper we highlight two prominent occasions where the occurrence of solibores are evident as a strong temperature front at the seabed and which are followed by, on the first occasion, a turbulent intrusion of cold, dense water with wave-like features on the density interface and, on the second occasion, a wave train whose structure is consistent with a dispersive wave tail. The period separating the two events is ~4 days, and in conjunction with the large scale currents, suggests that they are not forced by the tide despite being in a region where an internal tide is known to exist (Sherwin, 1991). We seek to establish to what extent the solibores are consistent with the results above for shoaling ISWs or overturning hydraulic jumps given their proximity to the seabed, and their likely forcing mechanism. Section 2 outlines the study region and the instrumentation deployed before the results from the field study are presented in Section 3. In Section 4 the cause of the solibores and their implications for near-bed mixing and transport processes over slopes are discussed before conclusions are made in Section 5.

2. Study region and instrumentation

2.1. Study region

Observations were conducted in the Faeroe-Shetland Channel (FSC) during the multi-disciplinary project, Processes over the Continental Slope (PROCS). The aim of PROCS was to study mixing processes over the continental slope, particularly those due to internal wave interactions with the sloping topography, and the influence these have on the cross-slope zonation of sediment

and benthic fauna. A cruise, PROCS 99-1, was conducted in 1999 during the period 14 April–5 May. A variety of moorings were deployed during the cruise and during a subsequent 'long term' 4-month period (PROCS 99-2). Given the predominantly cross-slope nature of the processes to be studied, particularly the internal tide, the moorings were deployed along a transect perpendicular to the continental slope on the southern side of the FSC (Fig. 1) between depths of 471–1000 m (Fig. 2). Given the prominence of the slope in influencing the physical regime, we adopt the standard convention of redefining our axes in the long-slope and cross-slope directions. Positive long-slope (y), referred to throughout the paper as a poleward long-slope flow (V), is defined as a heading of 52°N (True North), whilst positive cross-slope flow (x), referred to as up-slope flow (U), is defined as a heading of 142°N. The vertical coordinate is taken opposite to the direction of gravity, vertically upward from the bottom ($z = 0$ m).

2.2. Instrumentation

Table 1 summarises the details of the instrumentation used and the location of each mooring. Both traditional rotor and vane-type (Aanderaa RCM-8) and acoustic current meters (Aanderaa RCM-9) were mounted on the short-bottom moorings (c3, c5, c6, c8) at $z = 8$, 21, 34 and 47 m. The mechanical current meters exhibited short-period reductions in current speed which have been shown to be most likely caused by turbulence in the near-bed region (Hosegood and van Haren, 2003), and it is the unusually fast sampling of once per minute that provided such clear evidence of the solibores studied in this paper. Optical backscatter sensors (OBS) and sediment traps also measured the light transmittance and sediment fluxes at $z = 2$ and 30 m. A long ranger 75 kHz ADCP (LR-ADCP) was deployed at intermediate positions over the slope (b4), sampling current speed throughout the lower

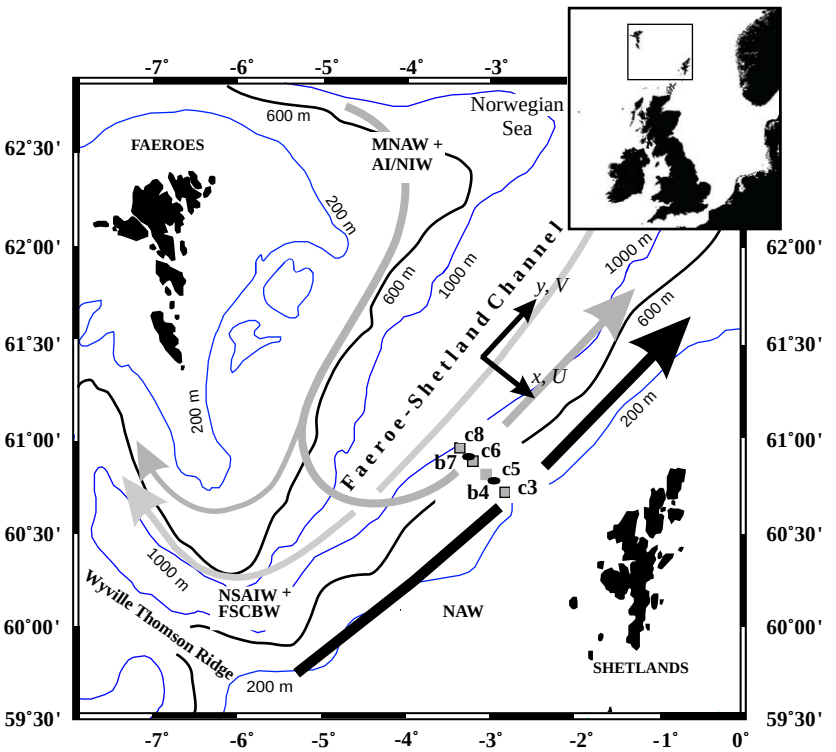

Fig. 1. Map of study region, indicating position of moorings over the slope and the principal water masses that flow through the FSC (see Turrell et al. (1999) for details on hydrography of FSC).

~300 m of the water column. High resolution measurements of current velocity and temperature were enabled by the use of a 600 kHz ADCP and NIOZ thermistor string (van Haren et al., 2001) at 494 m depth (a2).

In addition to moored in situ measurements, two CTD, OBS and Fast Light YoYo (FLY II) free-falling microstructure probe (Dewey et al., 1987) transects were conducted across the channel. At each station the FLY cast followed the CTD cast by ~30–60 min, depending on the water depth. Thus whilst the time interval between casts is relatively short, they should not be considered simultaneous, in particular given the timescale of the phenomenon studied here. We refer briefly to the results obtained from the long-term moorings. The majority of these moorings were lost due to fishing activity so that data is limited to the LR-ADCP at 850 m and sediment traps at 800 and 1050 m.

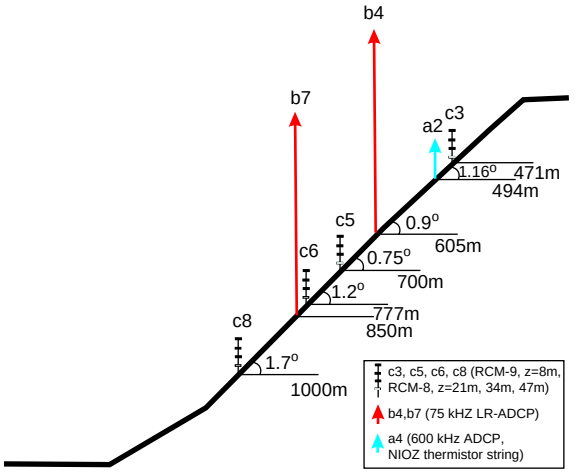

Fig. 2. Schematic of mooring locations over the slope.

3. Observations

In this section we present observations of the two solibores observed travelling up the Shetland slope during PROCS 99-1 on days 112 and 116 and to which we refer throughout the paper as the S1 and S2, respectively. Consideration is given to a third signal (S3) in the currents only at the deeper moorings and which is suggestive of a similar event on day 108. Due to the lack of a definitive temperature signal, however, we do not dwell in detail on S3.

3.1. Temperature and current variability over the slope

The leading edge of solibores S1 and S2 on days 112 and 116 are observed as strong temperature

Table 1
Summary of instrumentation employed during PROCS 99-1(c3, c5, c6, c8, a2, b4) and PROCS 99-2 (d3, d5, b4), between days 108–120 and 120–260, respectively

Mooring and position	Instrument	Depth (m)	Height above bottom, z (m)	Sampling interval (s)
c3	RCM-9, -8, -8, -8	471	8, 21, 34, 47	60
60°49′N, 2°59′W	OBS, PPS $\frac{3}{4}$ trap		2, 30	240, 1 day
a2	RDI 600 kHz ADCP	494	3–30, 0.5 m bins	30
60°49′N, 3°00′W	NIOZ thermistor string[a]		2–33, 1 m intervals	30
b4	RDI 75 kHz ADCP	605	17–357	300
60°53′N, 3°06′W			4 m bins	
d3, 5 (long-term mooring)	PPS $\frac{3}{4}$ trap	800, 1050	2, 30	11 days
60°57′N, 3°14′W; 61°00′N, 3°19′W				
b7 (long-term mooring)	RDI 75 kHz ADCP	850	17–357	600
60°58′N, 3°15′W			4 m bins	

All Aanderaa RCMs were equipped with temperature sensors.
As c3: c5, 700 m, 60°55′N, 3°11′W; c6, 777 m, 60°57′N, 3°13′W; c8, 1000 m, 61°00±N, 3°18′W.
CTD: SeaBird 911.
Microstructure: FLY II free falling probe.
[a]van Haren et al. (2001).

fronts marking the leading edge of the solibores at 471 m, with drops in temperature at $z = 8$ m of 4.47 °C in one minute and 0.9 °C in 10 min (decreasing by 1.674 °C in 51 min) for S1 and S2, respectively (Fig. 3A). There is no temperature signal attributable to either S1 or S2 at the deeper moorings due to their position below the thermocline where the temperature is comparatively uniform in the range $-1\,°C < T < 0\,°C$. Over the ~4 day period prior to day 112, the temperature at $z = 8$ m at 471 m is observed to rise almost monotonically from ~7 °C to a value of 8.377 °C before the drop attributed to S1. Following S1, the temperature again rises during a ~4 day period until S2 to 7.461 °C, when it again drops suddenly with the passage of a solibore.

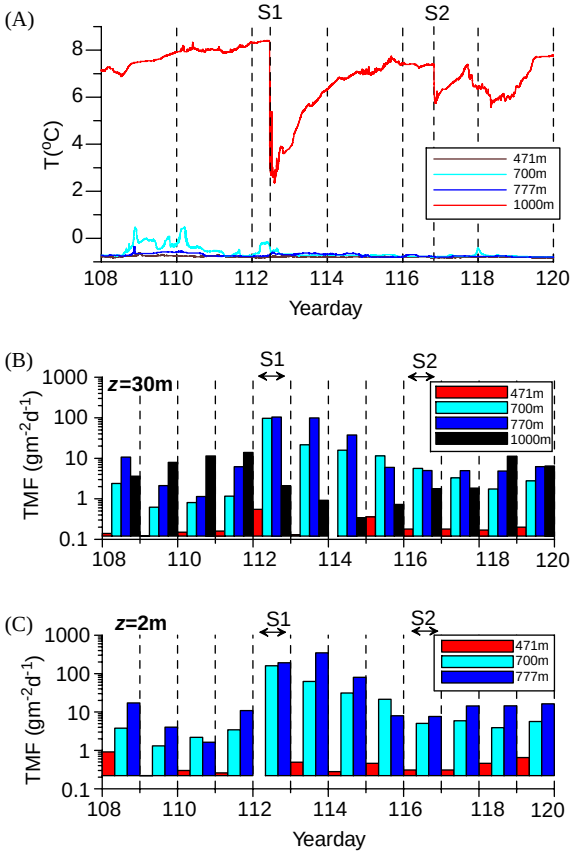

Fig. 3. (A) Temperature from $z = 8$ m, and sediment fluxes from (B) $z = 30$ m and, (C) $z = 2$ m, at 471, 700, 777 and 1000 m. S1 and S2 refer to the times of arrival of the solibores at 471 m.

The sediment fluxes at $z = 30$ m (Fig. 3B) indicate the coincident increase in resuspension associated with the passage of S1, particularly at 700 and 777 m. The largest observed total mass flux (TMF) of 350 g m^{-2} d^{-1} occurs at $z = 2$ m at 777 m on day 113 and is $O(10^2)$ larger than the background values. The time lag between S1 and the maximum sediment flux at this position is presumably due to the settling out of sediment brought into suspension, but the large fluxes at $z = 30$ m indicate the energy and particle motion associated with the solibore was sufficient to enable its upward mixing rather than simple resuspension and settling in the near-bed region.

The passage of S1 in a predominantly upslope direction is implied by the particle velocities measured at $z = 8$ m at 471 m (Fig. 4A); as it passes through the mooring, the cross-slope velocity reverses within ~10 min from a down-slope orientation with an amplitude of > 20 cm s^{-1} to an up-slope direction with a maximum amplitude of 52 cm s^{-1}. During S2 the cross-slope velocity is intensified in the up-slope direction, increasing from a velocity of 10 cm s^{-1} to a peak magnitude of 31 cm s^{-1} within a similarly short-time scale to S1. The only noticeable signal in the cross-slope velocity component at the deeper moorings is the strong reversal at 777 m during S1 from a down-slope flow of 43 cm s^{-1} to an up-slope flow of 35 cm s^{-1} (Fig. 4C), albeit over a slightly longer timescale of ~60 min compared to that at 471 m. A sharp but relatively small drop in the down-slope velocity at 700 m (Fig. 4B) occurs at S1, but is not so pronounced as the signals at either 471 m or 777 m.

The long-slope flow (Figs. 4E and F) is noticeable for the distinct reversal during S1 from an equatorward flow to a poleward flow at 700 and 777 m. The mean flow below the pycnocline is equatorward, so that the reversal during S1 represents a departure from the typical flow. At all depths other than 1000 m the passage of S1 is marked by a poleward surge, whereby the long-slope velocity component increases in strength and persists for a considerable length of time relative to the time-scale of the solibore itself. At each three locations the poleward surge is maintained over a period exceeding 18 h and for nearly 3 days at 471

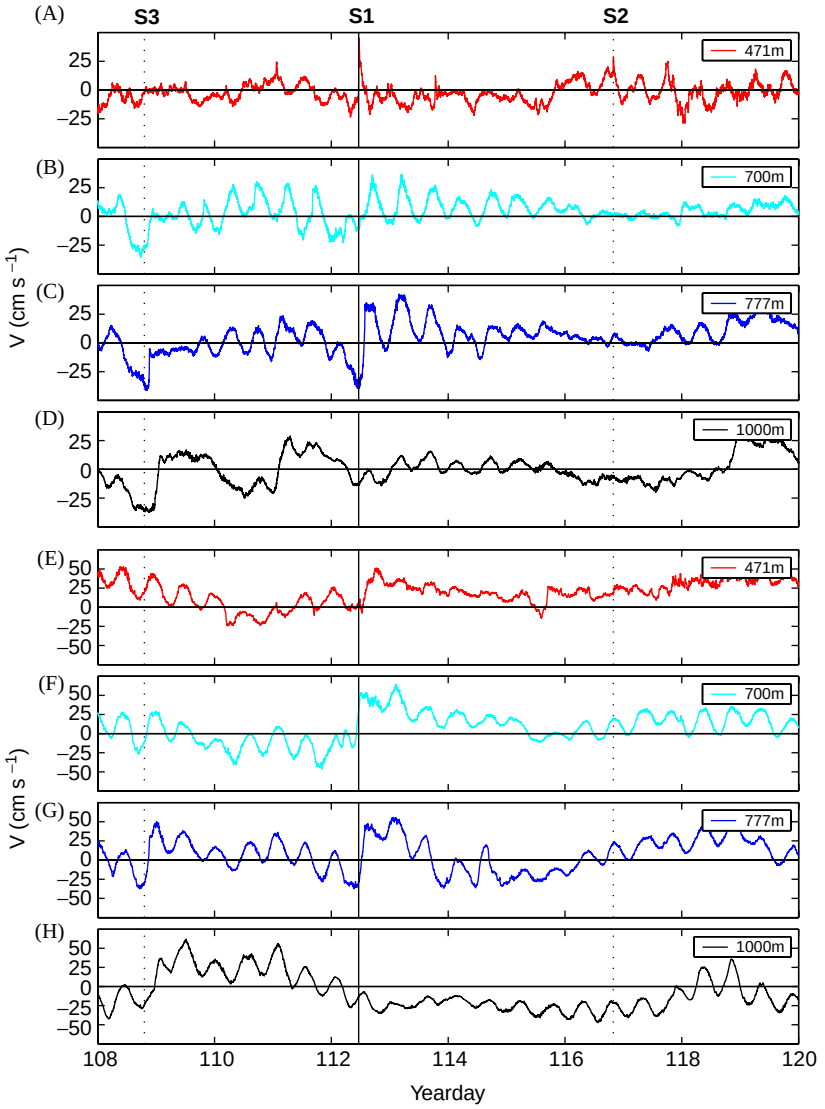

Fig. 4. (A–D) Cross-slope velocity and, (E–H) long-slope velocity from $z = 8$ at 471, 700, 777 and 1000 m. Data are smoothed with a 5-point running mean filter.

and 700 m. Fig. 5 illustrates the subinertial flow at $z = 8$ m at all moorings. The poleward surge following S1 is clear at 471, 700 and 777 m but not 1000 m. The long-slope velocities again turn poleward at the time of S2, although more gradually than during S1. The largest variance is observed at the mid-depth moorings at 700 and 777 m where the flow direction is influenced by the position and depth of the thermocline. It is again clear that 1000 m is out of phase with the shallower moorings.

We have previously suggested that a solibore may have also appeared over the slope on day 108 (S3) despite the lack of any distinct signal in the temperature records at 471 m where the solibores are most apparent due to the strong temperature gradients. We expect that, at the time of S3, the thermocline was constrained at a position over the

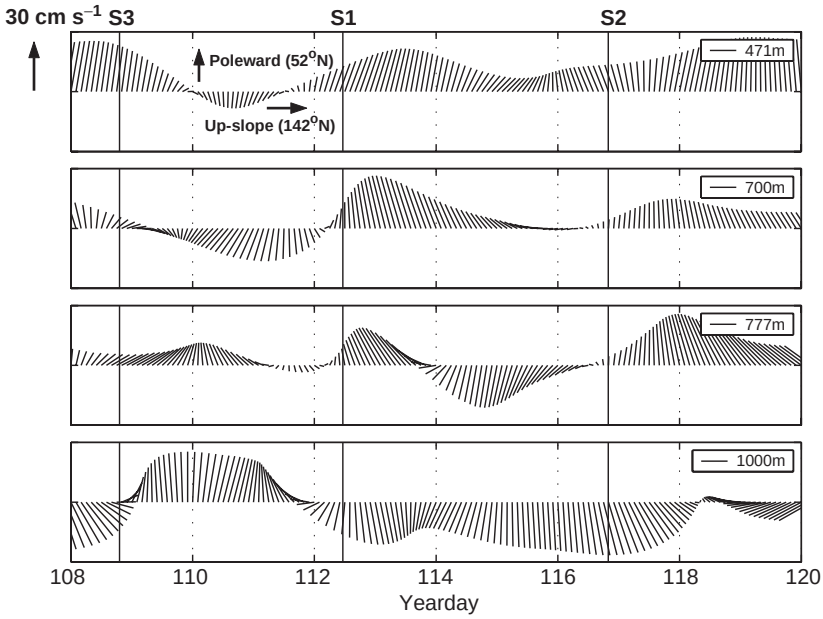

Fig. 5. Low-pass filtered (0.7 cycles/day cut-off) velocity vectors, instruments as in Fig. 4. Vectors are plotted every 2 h.

slope between a2 (494 m depth) and c5 (700 m depth), and that as a result there were simply no temperature sensors available to sample the well-defined temperature gradients so clearly observed during S1 and S2. Sharp gradients in both velocity components at 700, 777 and 1000 m during day 108 are similar to those at 777 m during S1, with the down-slope component at each three locations exhibiting a sudden drop in amplitude of $\sim 30\,\mathrm{cm\,s^{-1}}$ and the poleward surge evident as the long-slope component at 777 m again reverses rapidly from an equatorward flow to a poleward orientation with amplitudes in each direction $> 25\,\mathrm{cm\,s^{-1}}$.

3.2. Current variability with depth at mid-slope

An indication of the mid-slope barotropic currents is obtained by depth averaging the currents over the LR-ADCP range (Fig. 6), although by not reaching the surface the estimate should not be taken as a true value of the barotropic signal. Although S1 is evident as a period of strong currents near the sea-bed ($z < 50$ m) (Figs. 6A and C), it occurs during a barotropic neap tide (Figs. 6B and D), with S2 occurring as spring tide is approached. Near-bed currents at the sea-bed during S2 and S3 are intensified in the long-slope component but not to the same extent as during S1. The core of up-slope, poleward velocities during S1 is trapped within $z < 50$ m, extending upwards to a height of 150 m during day 113 before the signal becomes lost in the background field (Figs. 6A and C). The peak long-slope velocity of $45\,\mathrm{cm\,s^{-1}}$ during S1 leads that at 471 m by approximately 5.3 h whilst the aforementioned poleward surge following S1 is again clear at 605 m on day 112.31.

3.3. Temperature, turbulence and turbidity over the slope

We were fortunate to be conducting a CTD and FLY transect at the time of S1 and were thus able to capture, to a large extent, its passage up the slope and the associated enhanced turbulence it generated (Fig. 7A). A second transect was conducted 3 days later just before S2 and indicates conditions considered more typical of the region (Fig. 7B), but unfortunately prohibits a direct

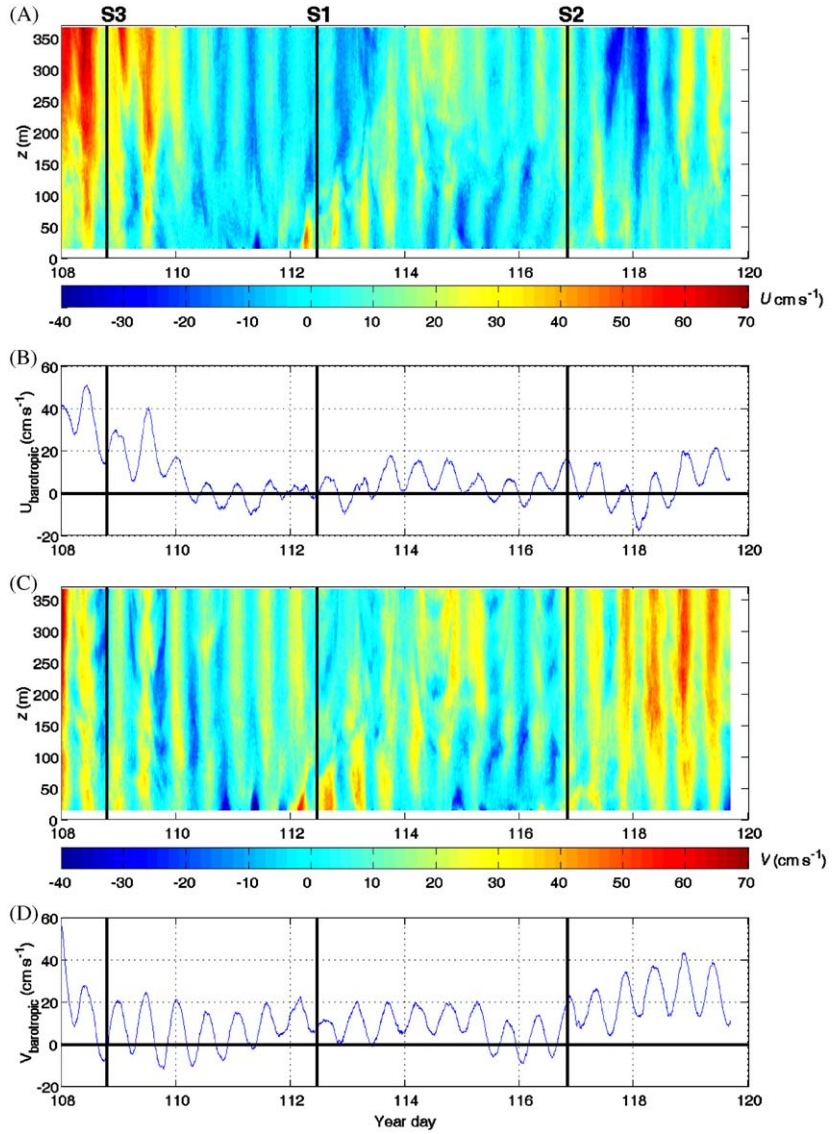

Fig. 6. (A) Cross-slope and (C) long-slope velocity from 75 kHz ADCP at 605 m, and (B) depth-averaged (approximation to barotropic currents) U and (D) depth-averaged V.

comparison of the temperature fields and associated turbulence between S1 and S2 due to the second transect being conducted before, rather than during, the passage of the solibore as was the case for S1. S1 is obvious as an intrusive thin layer (extending to $z = 50$ m) of cold water ($<4\,^{\circ}$C) extending up the slope. The intrusion extends from a depth of $\sim$600 m where the thermocline approaches the slope before running parallel with, and finally intersecting, the slope at a depth of $\sim$500 m. Rates of dissipation of turbulent kinetic energy, ε, typically exceed $10^{-7}\,\mathrm{W\,kg^{-1}}$ in the vicinity of the intrusion. Near the bed they exceed $0.5 \times 10^{-6}\,\mathrm{W\,kg^{-1}}$. The region of enhanced turbulence extends from the sea-bed to the upper edge of the thermocline where the strongest stratification

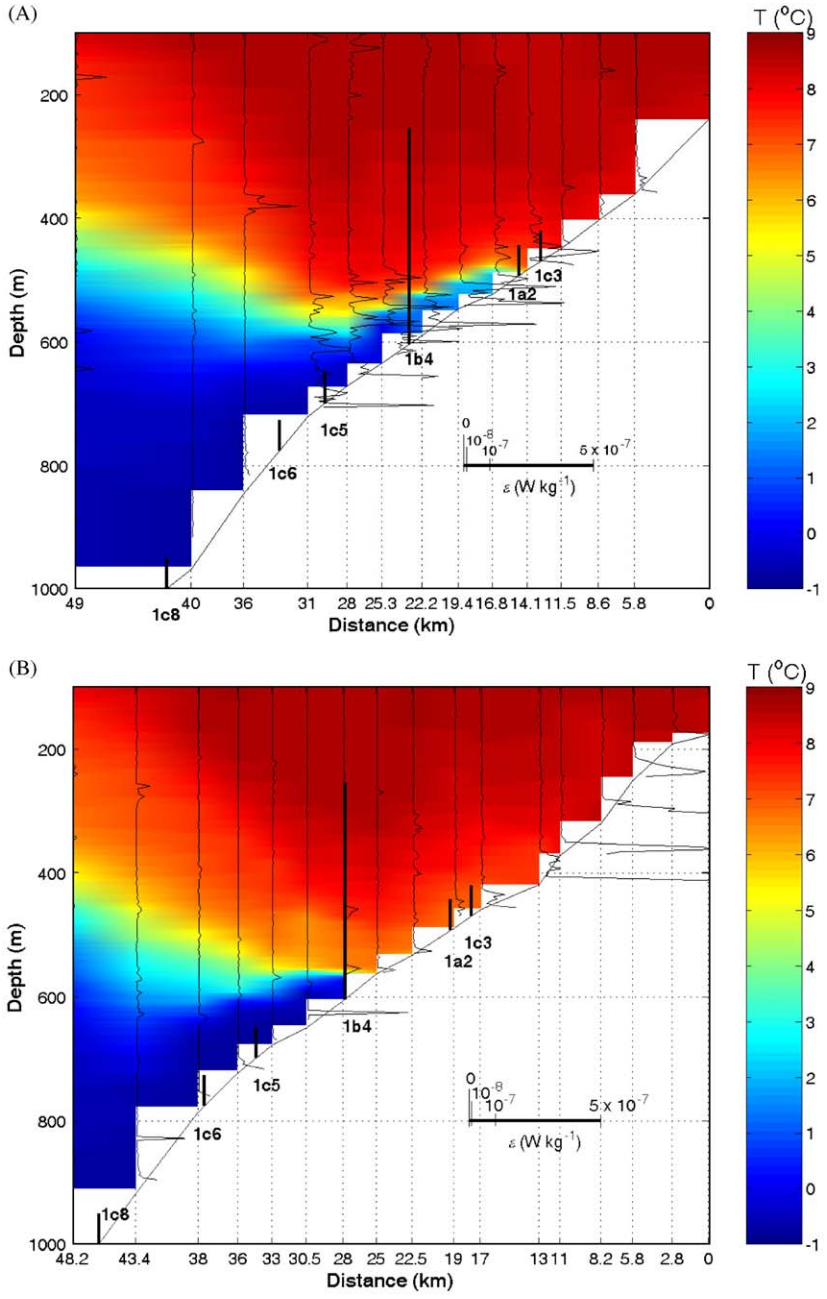

Fig. 7. Temperature and kinetic energy dissipation rate profiles conducted during PROCS 99-1; (A) Transect 1, days 111.97–112.68, and (B) Transect 2, days 116.19–117.06. Profiles were conducted at the specified distances, taken arbitrarily from the shallowest CTD profile.

enhances shear and thus potentially shear instabilities. The weaker stratification near the bed and high values of ε facilitates large vertical eddy diffusivities, $K_z = 0.2\varepsilon/N^2$ (Osborn, 1980). A maximum of $K_z \approx 10^{-1}\,\mathrm{m^2\,s^{-1}}$ is observed at $z = 10\,\mathrm{m}$ at 620 m, whilst K_z at $z < 30\,\mathrm{m}$ is consistently

$>10^{-4}\,m^2\,s^{-1}$. In contrast, the second transect indicates a relatively horizontal thermocline impinging on the slope at a depth of ~550 m and accompanied by low levels of $\varepsilon \approx O(10^{-9})\,W\,kg^{-1}$ (the noise level of this FLY) in the near-bed region within the vicinity of the thermocline. A zone of enhanced resuspension can be clearly seen at a depth of 600–700 m during the first transect (Fig. 8), correlating well with the sediment trap data indicated in Fig. 3.

3.4. High-resolution observations of two different solibores, S1 and S2

In this section we focus on the high-resolution measurements enabled by the use of the thermistor string and ADCP on mooring A2 at 494 m depth. We treat the two distinct solibores separately, beginning with S1 on day 112, before describing the different form of S2 on day 116.

3.4.1. S1

The strong temperature front associated with the leading edge of S1 is seen to extend to over $z = 32$ m at 494 m (Fig. 9A). The largest temperature gradient, $dT/dt_{max} = -2.24\,^{\circ}C\,min^{-1}$ is observed at $z = 2.5$ m, whilst at $z = 32$ m, dT/dt_{max} is reduced to $-0.699\,^{\circ}C\,min^{-1}$ at the leading face. The initial front is followed by a packet of approximately 5 waves supported by the strong stratification as indicated for reference by the 6 °C isotherm in Figs. 9B–D and which signifies the thermocline separating the cold (<5 °C) water typical of the intermediate waters in the FSC from the warmer (~7–8 °C) surface waters. The waves are asymmetric and extend upwards into the thicker (450 m) overlying layer. Amplitudes (measured from the preceding trough to the maximum displacement of the 6 °C isotherm) $\eta = O(10\,m)$, the largest being wave 5 with $\eta = 19$ m (Table 2). Periods are $O(30$ min), with corresponding lengthscales of 174–319 m assuming a constant phase speed, c, of 24 cm s^{-1}, determined by the difference in times of arrival of the temperature front at 494 and 471 m of 81 min. This estimate of phase speed is only valid on the assumption that the particle velocities in the wave front are in the direction of propagation, as is the case for ISW, and that the solibore is thus travelling directly up the slope. Taking this assumption to be valid, the calculation of the phase speed is able to be determined accurately

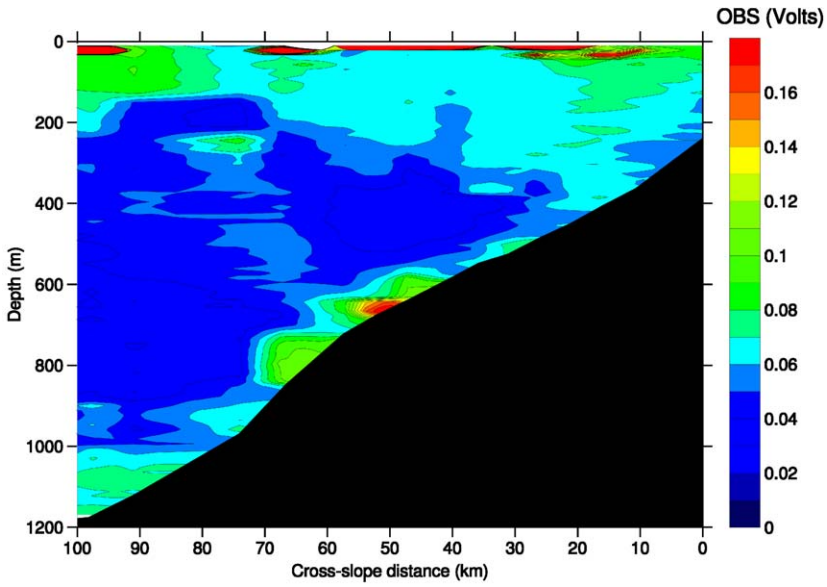

Fig. 8. Light attenuation, measured by the OBS mounted on the CTD frame, during Transect 1 and indicating the core of turbidity associated with S1.

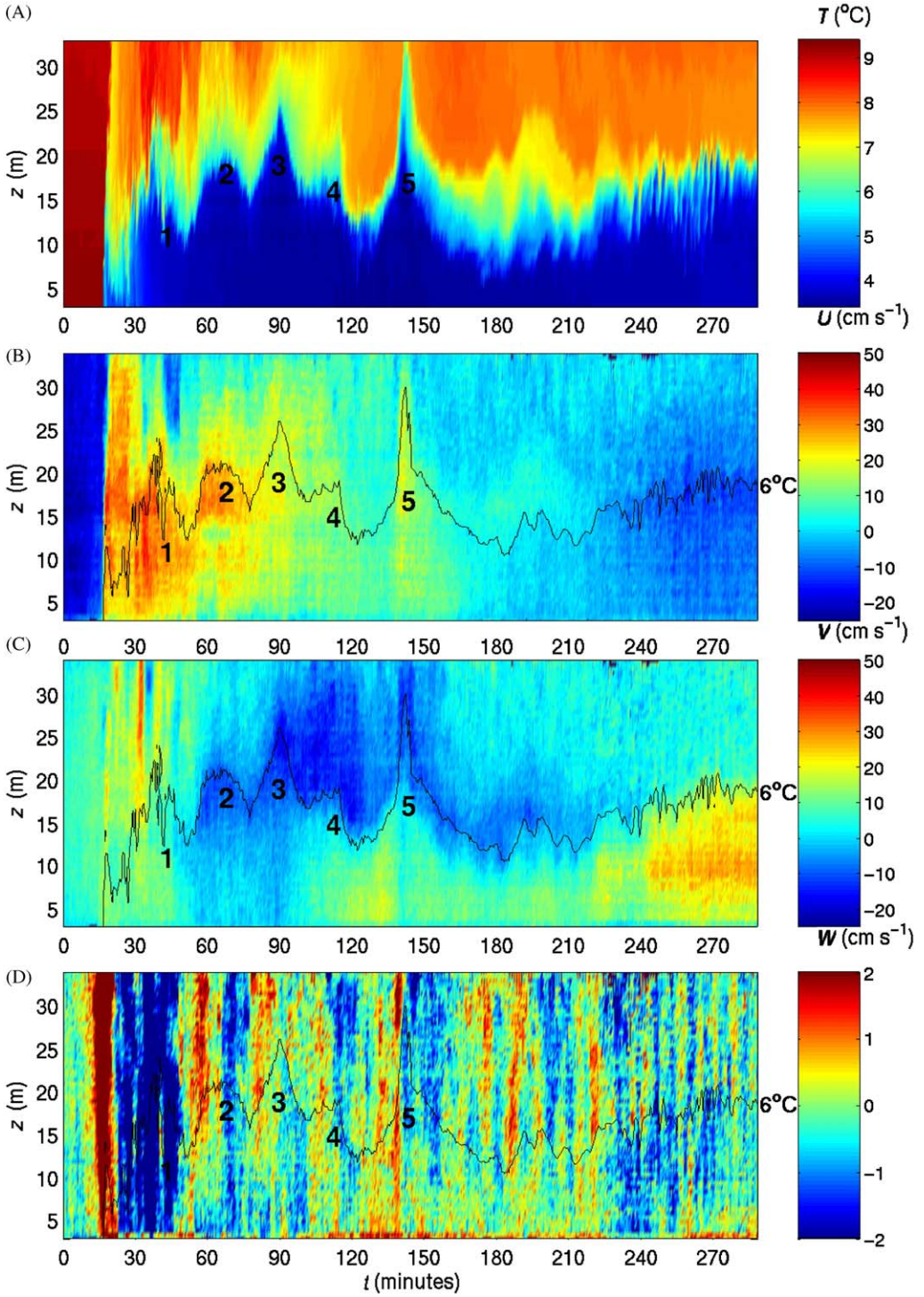
(A)
T (°C)
z (m)
U (cm s−1)
(B)
6°C
V (cm s−1)
(C)
W (cm s−1)
(D)
t (minutes)
1
2
3
4
5

Table 2
Wave characteristics, S1

Wave	Amplitude, η (m)	Wavelength, L, at 0.42η (m)	Period, T (min) at 0.42η
1	18.2	319	20
2	9.2	301	20
3	10.5	174	12
4	7.9	217	14
5	19.1	143	10

The amplitude, η, is defined as the maximum vertical excursion of the 6 °C isotherm from the position of the preceeding trough. Horizontal wavelength is defined as the distance between points on the leading and trailing edges of the wave where the 6 °C isotherm is displaced by $0.42 \times \eta$ (e.g. Osborn and Burch, 1980). Wavelengths are calculated on the premise of a phase speed, $c = 0.25\,\mathrm{cm\,s^{-1}}$.

due to the strength of the temperature gradients being such that the time of arrival of the solibore is able to measured to within a minute corresponding to the instruments sampling period. A further property of an internal bore is that the linear long-wave phase speed, c_{linear}, behind the bore exceeds the speed of the bore itself (Henyey and Hoering, 1997). An appropriate CTD profile, taken at 485 m during the passage of S1 and which indicates an approximately two layer system of two uniform layers separated by a strong density interface, is used to calculate the upper and lower layer densities and thicknesses, ρ_1, H_1 and ρ_2, H_2, respectively, to determine c_{linear}

$$c_{\mathrm{linear}} = \left[\frac{g' H_1 H_2}{(H_1 + H_2)}\right]^{1/2}, \qquad (1)$$

where $g' = g(\rho_2 - \rho_1)/\rho_2$. We find for $\rho_1 = 1027.43\,\mathrm{kg\,m^{-3}}$, $H_1 = 450\,\mathrm{m}$, and $\rho_2 = 1027.95\,\mathrm{kg\,m^{-3}}$, $H_2 = 100\,\mathrm{m}$, $c_{\mathrm{linear}} = 0.64 \pm 18\,\mathrm{cm\,s^{-1}}$; a thinner lower layer reduces c_{linear}. Thus S1 appears to satisfy the definition of an internal bore.

The velocity field is characterised by a core of enhanced up-slope velocity at $15 < t < 90$ min (Fig. 9B) reaching a maximum of $U = 52\,\mathrm{cm\,s^{-1}}$ at $z = 16$ m at the leading edge. The front is characterised by a zone of strong convergence, with a down-slope flow immediately preceding the solibore. Superimposed on the core of enhanced velocities are the wave-induced particle velocities, which are most clearly observed during the passage of waves 2 and 5 as perturbations in the up-slope direction. During the passage of wave 5 the cross-slope velocity increases from approximately 0 to $>20\,\mathrm{cm\,s^{-1}}$ at $z = 15$ m. The long-slope velocities are comparatively low (Fig. 9C) implying a principally up-slope propagation of S1 if assuming particles velocities are in accordance with those expected for ISWs and further suggested by the time lag between the arrival of the temperature front at 494 and 471 m. The surge in long-slope velocity emerges in the bottom layer at $t = 100$ min, extending upwards away from the bed with time. In contrast long-slope velocity above the interface is directed equatorward. Strong upward vertical velocities are evident in the convergence zone at the leading edge of S1 at $t = 15$ min and extend beyond $z = 32$ m (Fig. 9D). A maximum value of $W = 16.2\,\mathrm{cm\,s^{-1}}$ is observed at $z = 16$ m and is followed by strong downward velocities which persist until $t = 55$ min; thus the leading edge forms a rotor such as proposed by Thorpe (1998) to occur for shoaling internal waves in a lake and whose flow is contrary to the forward breaking of a surface wave. A series of oscillations may then be discerned with typical velocities of $O(2\,\mathrm{cm\,s^{-1}})$ and which correlate with the position of isotherm displacement associated with the waves; upwards (positive) vertical velocities are found at the leading edge of the waves and downwards (negative) velocities at the trailing edge. Note that the vertical velocity oscillations extend to the lowest height above the seabed we were able to measure at $z = 2$ m.

Fig. 9. (A) Temperature, (B) cross-slope, (C) long-slope and (D) vertical velocities during S1 as measured at pro1a2 (494 m). Temperature is measured by the NIOZ thermistor string (van Haren et al., 2001), $z = 2-32$ m, velocity by the 600 kHz ADCP mounted at $z = 2$ m. The time origin is taken arbitrarily just before the initial temperature front. Numbers corresponding to individual waves are referred to in the text. The colour scale in (D) is compressed within the maximum and minimum values of W in order to highlight the oscillations in the wave train following the initial rotor.

The density at 494 m is calculated by establishing a temperature–salinity relationship from the CTD profile conducted during the passage of S1 at a depth of 524 m. The station was chosen to ensure the T–S relationship is suitable for the range of temperatures sampled during the passage of the solibores, approximately $3 < T < 8\,^{\circ}\mathrm{C}$ (Fig. 10). A fifth-order polynomial is fitted to the CTD data and the coefficients used to evaluate the density from the thermistor string data and from which the buoyancy frequency is calculated

$$N = \left(-\frac{g}{\rho_0} \frac{\Delta\rho}{\Delta z} \right)^{1/2}, \tag{2}$$

where g is the gravitational acceleration, ρ_0 is a reference density and $\Delta\rho$ the change in density over a depth interval, $\Delta z = 5$ m. A maximum of

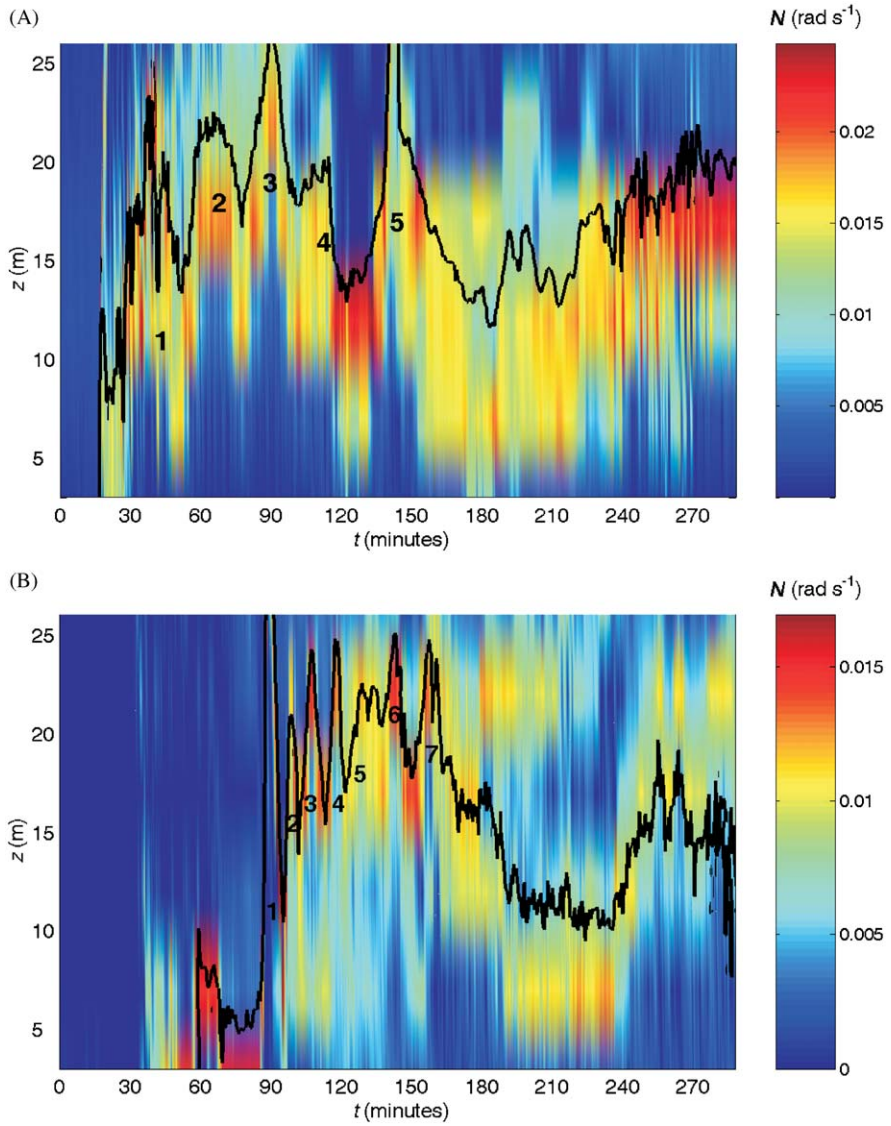

Fig. 10. Buoyancy frequency, N (rad s^{-1}) during (A) S1 and (B) S2. Note the different colour scale used; N was calculated over a vertical distance, dz, of 5 m for each one minute time step.

$N = 2.5 \times 10^{-2}\,\mathrm{rad\,s^{-1}}$ is observed in the trough preceding wave 5, with typical values of $O(10^{-2}\,\mathrm{rad\,s^{-1}})$ found along the thermocline which support the waves (Fig. 10A). At $t = 270$ min a region of strong stratification, with $N_{max} = 2.4 \times 10^{-2}\,\mathrm{rad\,s^{-1}}$, coincides with a packet of short-period oscillations, following which the depth of the thermocline rapidly shallows and inundates the thermistor string with the colder water. The corresponding buoyancy oscillation period is 260 s whilst the typical period of the high-frequency waves is 100 s; thus the waves have frequencies, $\sigma > N$, which is theoretically impossible given the allowable frequency range of internal gravity waves of $f < \sigma < N$. Two possibilities explain the apparently high frequency of these waves; firstly, the waves may be Doppler shifted to a higher frequency, in a similar manner to that suggested by Thorpe (1987), by the solibore itself due to it being a moving source. Secondly, the waves may be indicative of Kelvin–Helmholtz instabilities resulting from the shear across the density interface rather than being free internal waves. The latter is supported by the slightly tilted orientation of the waves with respect to the vertical, indicative of static instability, and, particularly in the case of the wave-like disturbances at $t = 180-210$ min and $z = 10$ m, 'claw' structures in the temperature record indicative of the formation of vortices at the interface. Thus the apparent waves towards the end of the solibore may actually be billows resulting from the enhanced shear.

3.4.2. High-resolution velocity and temperature measurements, S2

The waves during S2 are shorter but more distinct than S1, with a packet of approximately 7 led by a particularly large wave of amplitude $\eta = 30$ m (Fig. 10B, Table 3). The temperature gradients are weaker given $6\,^{\circ}\mathrm{C} < T < 8\,^{\circ}C$, with $\mathrm{d}T/\mathrm{d}t_{max} = -0.785\,^{\circ}\mathrm{C\,min^{-1}}$ at $z = 31$ m on the leading edge of wave 1. N is subsequently smaller, reaching a maximum of $1.69 \times 10^{-2}\,\mathrm{rad\,s^{-1}}$ (Fig. 10B). The wave train, defined by the displacement of the 7 °C isotherm, is more coherent than during S1, with waves 1–4 in particular displaying the sech^2 profile typical of ISWs (Fig. 11A). A short extension of strongly stratified ($> 1.6 \times 10^{-2}\,\mathrm{rad\,s^{-1}}$) fluid constrained at $z < 10$ m leads wave 1 at $t = 60-90$ min. The 'nose' is noticeable in the ADCP data as a sharp perturbation in both the cross-slope and long-slope velocities directed up-slope and poleward at $t = 30$ min, as opposed to the ensuing wave train which has perturbations principally in the long-slope component (Fig. 11B). Furthermore, and in contrast to S1, the wave train that trails the initial front is characterised by a core of enhanced velocity in a predominantly poleward direction (Fig. 11C), reaching $V = 40\,\mathrm{cm\,s^{-1}}$ between $120 < t < 180$ min, and with perturbations also in the poleward direction as opposed to the principally cross-slope direction of the wave-induced perturbations in S1. Waves 1–4 all exhibit particle velocities in accordance with ISW (see, for example, Osborn and Burch, 1980) of elevation propagating in an oblique but principally poleward direction; vertical velocities, W, are well defined although, as with S1, the magnitudes are relatively small of $O(2\,\mathrm{cm\,s^{-1}})$ following the leading front which forms a rotor in the same way as S1 (Fig. 11D). Maximum vertical velocities are nonetheless high, with $W = 14.5\,\mathrm{cm\,s^{-1}}$ observed at $z = 27$ m and a return downward flow of $-12.7\,\mathrm{cm\,s^{-1}}$ at $z = 22.5$ m. As opposed to S1 the vertical velocity oscillations are constrained to the vertical extent of the waves and do not extend below the interface to the sea-bed.

Table 3
As Table 2 for S2

Wave	Amplitude, η (m)	Period, T (min) at 0.42η
1	30	4
2	10.5	4
3	10.4	4
4	9.2	4
5	5.5	5
6	4.8	5
7	7.2	4

Wavelength is not given due to our inability to accurately determine the phase speed, c.

3.5. Long-term observations

We briefly summarise the pertinent results from the deep long-term moorings deployed for ~4

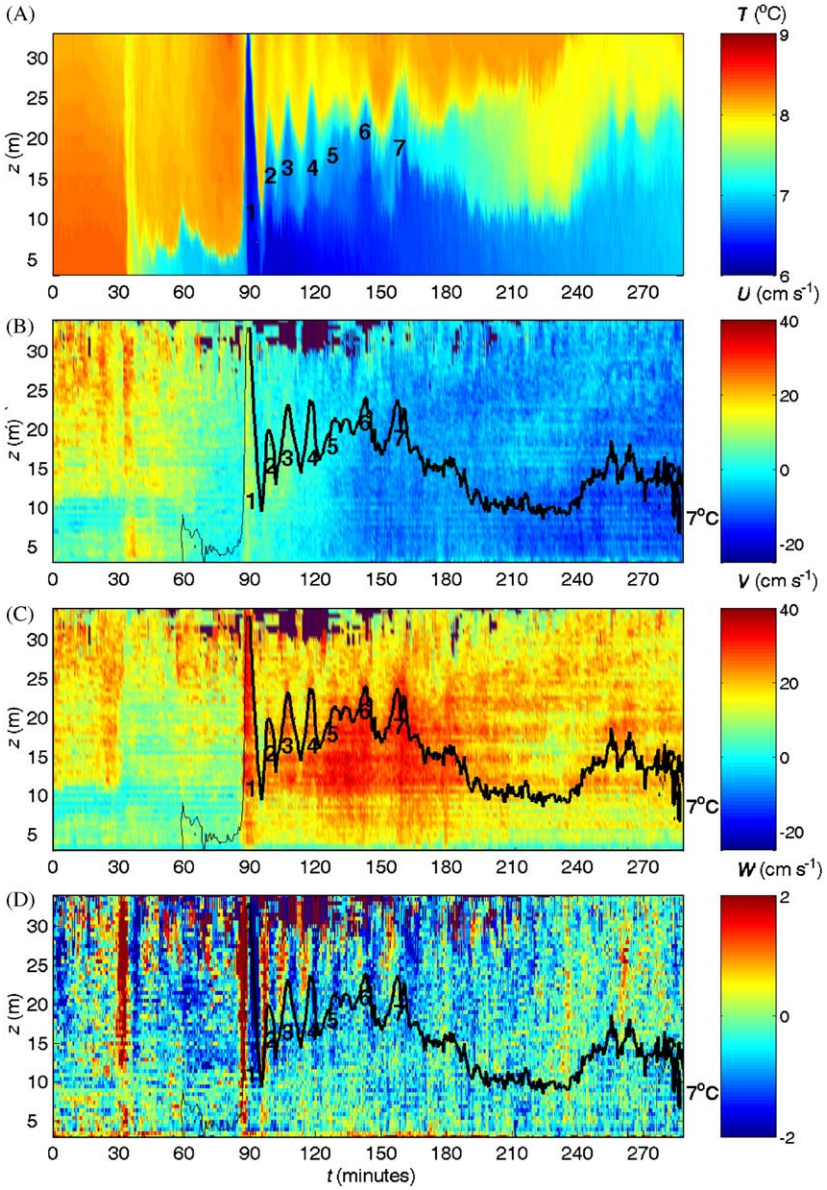

Fig. 11. As Fig. 9 during S2.

months between the two cruises. Spectra computed for each 4 m depth bin of the LR-ADCP deployed at 850 m indicate a concentration of sub-inertial energy between $100 < z < 200$ m at $\sigma \sim 0.35 \pm 0.04$ cpd, corresponding to a period of 2.84 ± 0.35 days (Fig. 12). The concentration of low-frequency energy around a depth of 700 m was also alluded to in Section 3.1 where largest variations were observed at 700 and 777 m. At all frequencies energy decreases towards the bed. The low-pass filtered (cut-off frequency = 0.7 cpd) velocity further demonstrates the existence of the sub-inertial variability in the bottom 300 m of the water column and the sharp gradients in both components that characterised the occurrence of S1 and S2 in the short-term moorings. The

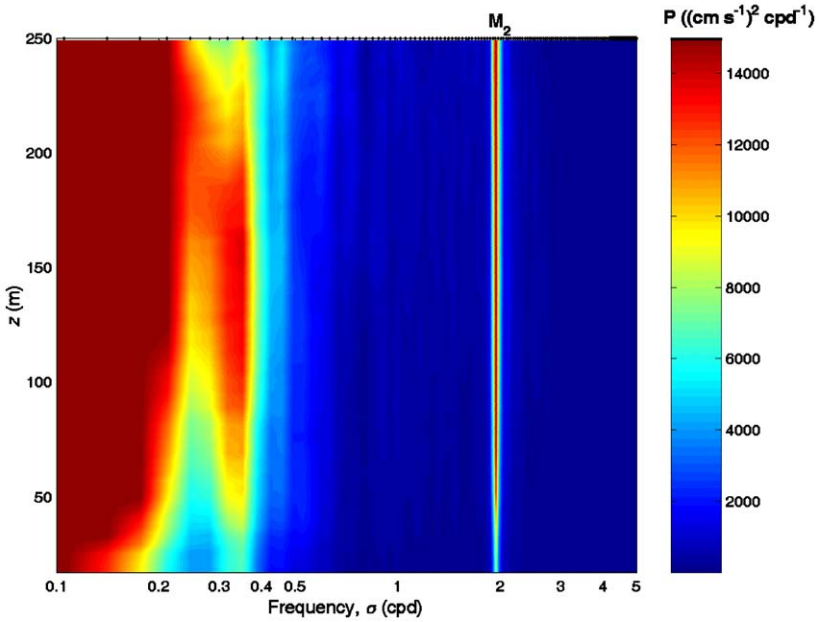

Fig. 12. Horizontal kinetic energy spectra (degrees of freedom = 17) for each depth bin ($dz = 4$ m) during long-term deployment, days 120–260, from 75 kHz ADCP at 850 m. Tick marks on the top y-axis represent the frequency resolution = 0.0352 cycles/day.

subinertial currents are not intensified at the bottom and there is no phase propagation in the strong signals, which appear to be related to the generation of solibores in the same way as S1 and S2 (Figs. 13A and B). Nonetheless, a period of hugely enhanced resuspension occurs during the period 153.5–164.5 when a flux of 94.14 g m^{-2} d^{-1} (averaged over 11 days) was observed at $z = 2$ m at 800 m (Fig. 13C). During this time the long-slope current reverses rapidly from a poleward to an equatorward direction. The change is as abrupt as during S1 but in the opposite sense. A second period of enhanced resuspension occurs at 1000 m during the period 197.5–219.5 when observed fluxes were 20.03 and 22.44 g m^{-2} d^{-1}; again the long-slope velocity exhibits an abrupt reversal but on this occasion in the same sense as S1, reversing from an equatorward to a poleward direction.

4. Discussion

On two occasions, S1 and S2, within a 12-day period we have observed thermocline intrusions upward along the sloping bottom of the FSC, accompanied by nonlinear waves. We describe them as solibores, implying they begin borelike before becoming more wavelike later in their evolution. Within this section we discuss the potential origin of the solibores and the reason for the differences between the two, their potential for influencing boundary mixing processes and sediment resuspension and redistribution at the continental slope. Finally we propose their potential forcing mechanisms.

4.1. Internal hydraulic jumps at the sea-bed

Holloway (1987) observed hydraulic jumps on the Australian North West Shelf resulting from the steepening of the leading face of an internal tide as it approached shallow water. The isotherms prior to a jump are bunched together indicating a strong stratification above a deep mixed layer, with strong flow directed offshore in the upper layer before rapidly swinging round to an onshore direction with the passing of the hydraulic jump. In our observations, the depression of the thermocline

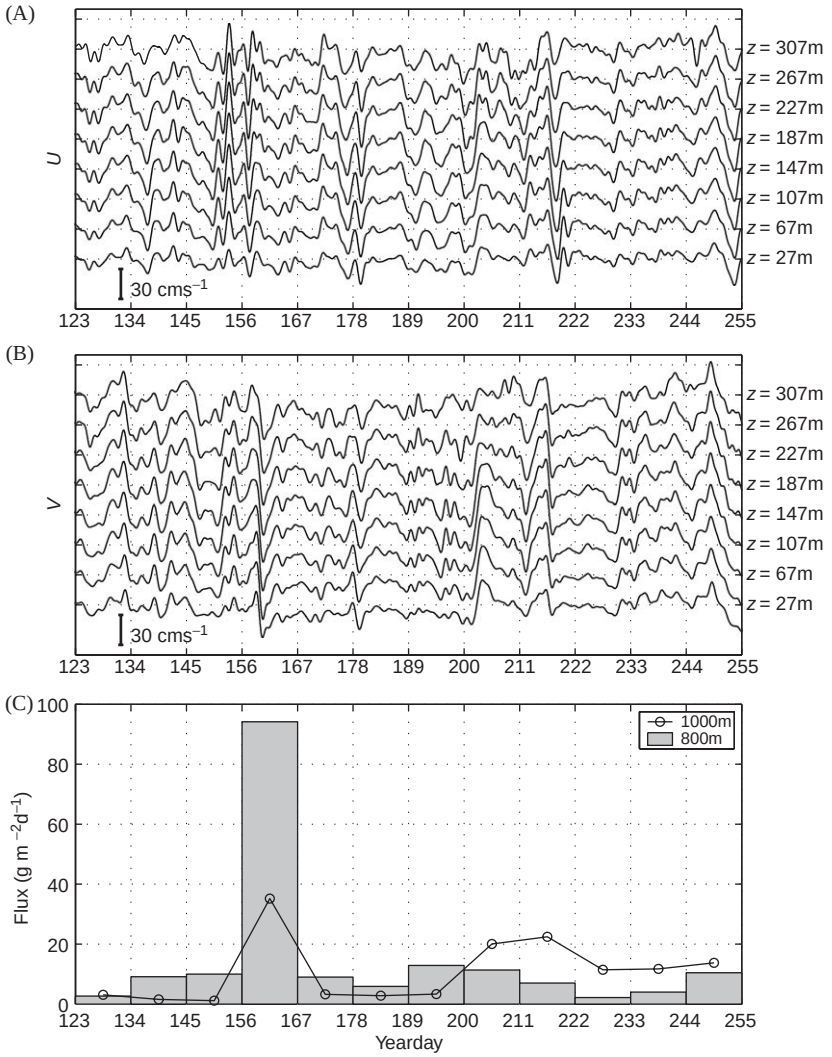

Fig. 13. Every 10th depth bin of low-pass filtered (cut-off frequency = 0.7 cycles/day) (A) cross-slope and (B) long-slope velocity sampled by 75 kHz ADCP at 850 m depth and (C) total mass fluxes measured by sediment traps at $z = 2$ m (800 and 1000 m), during long-term deployment. The velocity for each height is offset by $+30\,\mathrm{cm\,s^{-1}}$ from the previous record.

prior to S1 implies a strong, near-bed stratification, whilst on day 111.4 we observe a distinct pulse in down-slope, equatorward flow (Figs. 14C and D) near the bed at 605 m and which is immediately followed by a reversal in current direction to an upslope, poleward orientation. Fig. 6 indicates that the pulse is concentrated at the bottom and thus, we assume, represents flow in the lower layer below the pycnocline. We consider whether the pulse is sufficiently strong to cause a hydraulic jump.

Following Holloway (1987) but reversing the density interface to a near-bed position as opposed to a near-surface pycnocline, we define the nondimensional variables (see Fig. 15A)

$$\text{Layer height}: \quad R_1 = h_1/H; \quad R_2 = h_2/H,$$
$$\text{Velocity ratio}: \quad T_1^2 = u_1^2/u_2^2; \quad T_2^2 = u_2^2/u_1^2,$$

where h_1, h_2 are the upper and lower layer thicknesses, H is the total water depth and u_1, u_2

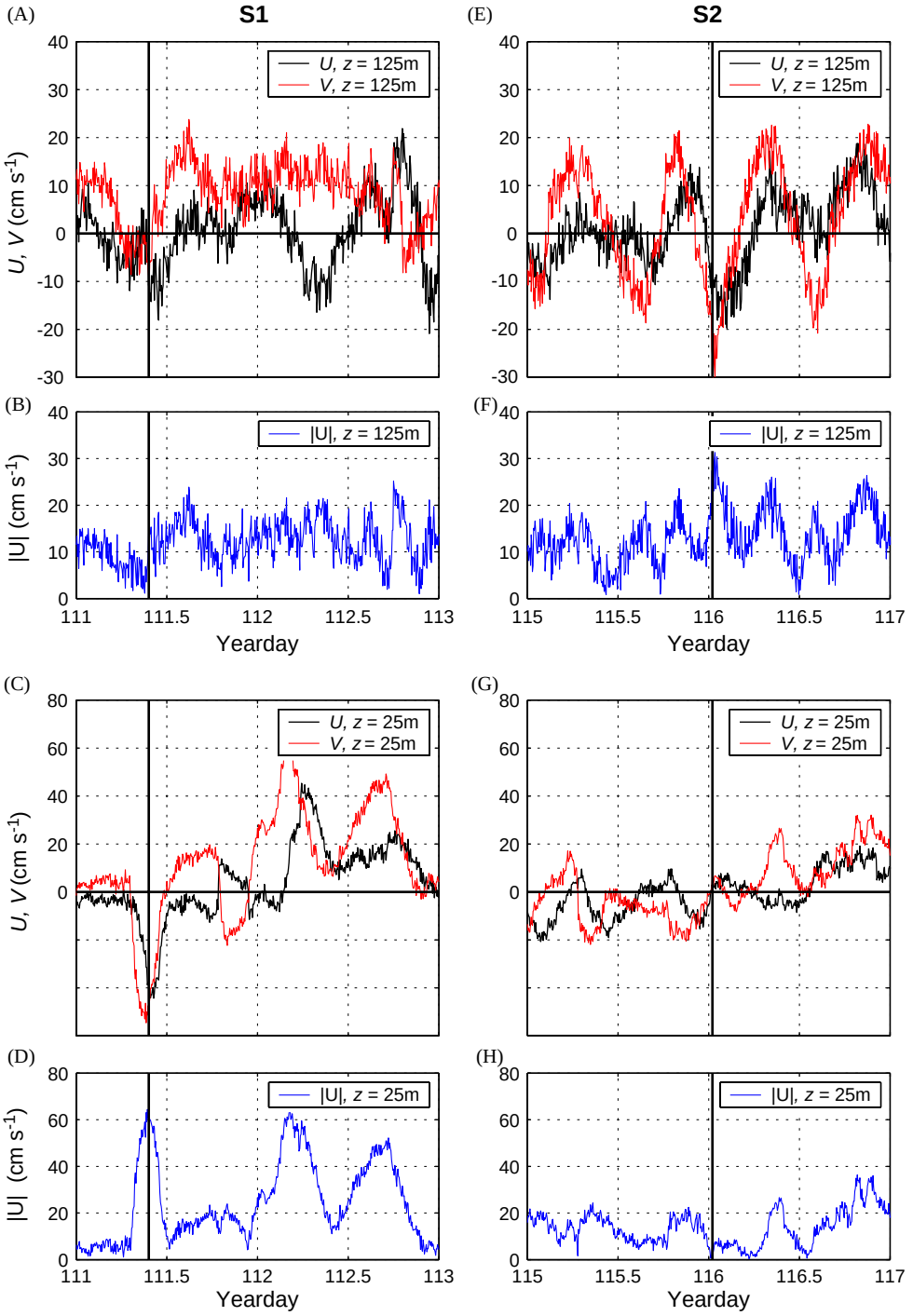

Fig. 14. (A) Cross-slope, U, and long-slope, V, velocity, and velocity amplitude, $|U|$ during S1 (A–D) and S2 (E–H) at $z = 25$ m and 125 m, 605 m depth. Solid vertical lines at year days 111.4 and 116.02 correspond to the times for which calculations of hydraulic conditions were made.

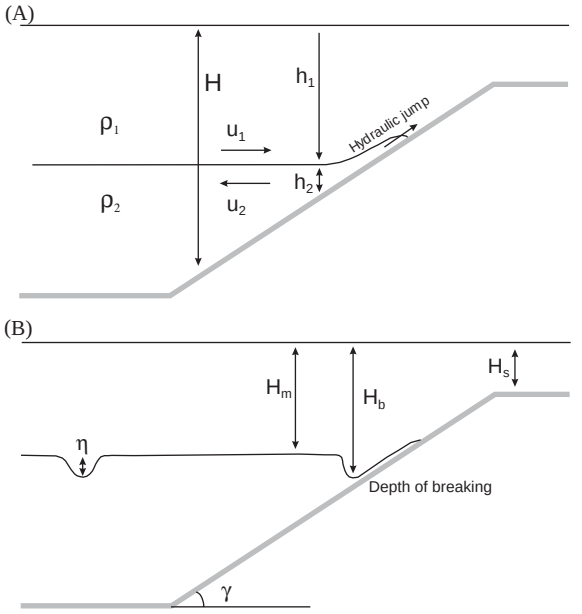

Fig. 15. Schematic of parameters used in: (A) hydraulic model and (B) model for shoaling ISWs.

are the upper and lower velocities, respectively. The Froude number, Fr, may be expressed as

$$Fr = \left[1 + \frac{RT^2}{1 - R^2}\right]^{-1/2}, \quad (3)$$

for which a jump is expected for hydraulically critical conditions when $Fr \leqslant 1$. Applying the observed values of u_1, $u_2 = 20$, $60\,\mathrm{cm\,s^{-1}}$, respectively, $h_2 = 50\,\mathrm{m}$, $H = 650\,\mathrm{m}$ and g' as calculated for (1), gives $Fr = 0.99$ applying R_2 and H_2 to give the lower layer Froude number. The low value of $R = 0.07$ ensures that $Fr \sim 1$ for a large parameter space, such that even for variations in T^2 hydraulically critical conditions are likely. Thus the pulse in down-slope, equatorward flow prior to S1 on day 111.4 seemed sufficient to create a hydraulic jump. Prior to S2 the temperature data across the slope imply the thermocline was not so depressed, but a pulse is observed at $z = 125\,\mathrm{m}$ with relatively quiescent conditions at $z = 25\,\mathrm{m}$. Applying R_1 and H_1 to give the upper layer Froude number because the strong flow is above the thermocline, $Fr = 0.89$ on assuming the same values of h_1 and h_2, again suggesting hydraulically critical conditions were achieved and promoting the development of a hydraulic jump. The orientation of the jump is not dependent on which layer is hydraulically critical, as confirmed by Holloway (1987) who found both upward and downward jumps for critical conditions in the upper layer alone.

Whilst the evolution of the internal tide across the Australian North West shelf as a hydraulic jump to an undular bore has been studied (Smyth and Holloway, 1988), the proximity of the hydraulic jump to the sea-bed means that a more suitable context within which to discuss our findings is the evolution of a baroclinic bore at the sea-bed, studied in laboratory and numerical experiments on shoaling ISWs over slopes. Vlasenko and Hutter (2002) (hereafter VH02) found that the *rear* face of an incident ISW of amplitude η steepens due to nonlinearity (Fig. 15B), forming a baroclinic bore which may then overturn due to kinematic instabilities. The overturned bore then transforms into a horizontal density intrusion propagating up the slope. For less steep slopes, however, the longer transition zone enables dispersion to balance nonlinearity and form a dispersive wave tail. A number of similarities exist between our observations over a sloping boundary in the ocean and the numerical results of VH02. The similarities we observe are

(1) A rotor is formed at the leading edge of the bore, with strong upward velocities followed by a region of downward velocities of slightly smaller magnitude (Figs. 9D, 11D; Figs. 3G–I in VH02).
(2) After breaking the ISW transforms into a horizontal density intrusion propagating onto the shelf, with a core of strong horizontal velocity in the direction of propagation (Figs. 9B, 11C; Fig. 7B in VH02).
(3) Wave-like structures appear along the upper edge of the density interface bounding the horizontal density intrusion, and are the result of the multiple reflections from the bottom following overturning (Fig. 9B; Fig. 7A in VH02). Such structures are also referred to as 'soliton-like waves of elevation' (VH02) or

turbulent boluses (Helfrich, 1992; Lamb, 2002).

(4) The effect of the multiple reflections from the sea-bed is a pattern of oscillating vertical velocities which extend to the sea-bed (Fig. 9D; Fig. 7C in VH02) rather than being constrained to the leading and trailing edges of genuine ISWs.

(5) For a gentle slope a dispersive wave tail, as is observed in S2, is formed rather than an overturning hydraulic jump (Fig. 11; Fig. 9 in VH02).

The parameters that describe the breaking event in the numerical studies of VH02 are unlikely to be obtained in the ocean with the required accuracy to make quantitative comparisons with the theory useful. This is the case here, where a lack of measurements in the far field and of high resolution measurements deeper than those obtained at 494 m and where the hydraulic jump is expected to have originated, render a determination of the ISW amplitude required for breaking to occur impossible. Furthermore, the aforementioned pulse in current speed prior to S1 in particular and the subsequent strong reversal in direction is not consistent with a shoaling ISW. However, the results of VH02 essentially relate to an overturning baroclinic bore and may be extended to the case of hydraulic jumps at the sea-bed resulting from other processes.

The importance of the bottom slope to the breaking process described in VH02 is useful to elucidate qualitatively the difference between the forms of S1 and S2. An ISW propagating from deep water into a region of sloping topography will break at the depth H_b (Fig. 15B), when the relationship

$$|a| = \frac{\eta}{H_b - H_m}, \tag{4}$$

where H_m is the undisturbed depth of the isopycnal exhibiting maximum displacement by the ISW and $|a|$ is the nondimensional wave amplitude, is satisfied by

$$|a| \cong \frac{0.8^\circ}{\gamma} + 0.4, \tag{5}$$

where γ is the angle of the bottom-slope (VH02). Thus as γ is reduced in (5), the magnitude of $|a|$ is increased, such that a larger initial wave amplitude is required for breaking to occur. The direction of propagation of S1 inferred from the particle velocities is principally up-slope along a bottom having an observed $\gamma = 1.16^\circ$, whilst the particle velocities of $>26\,\mathrm{cm\,s^{-1}}$ are greater than the speed of the bore which we calculate by comparing the time of arrival of the temperature front at 494 m and then at 471 m. This satisfies the kinematic instability mechanism for the overturning of a baroclinic bore according to Kao et al. (1985), Grue et al. (2000) and VH02 and explains the form of S1 being consistent with the results of VH02 for an overturned ISW (points 1–4 above). During S2, however, when the form of the solibore is more that of a dispersive wave train, the particle velocities imply a principally long-slope direction of propagation; at $t = 90$ min we observe $U = 9\,\mathrm{cm\,s^{-1}}$ and $V = 32\,\mathrm{cm\,s^{-1}}$, giving an angle between isobaths and the boundary projection of the group velocity vector, $\theta = 16^\circ$ (Fig. 16). The effective slope is thus reduced to $\gamma_{\mathrm{effective}} = \sin^{-1}(\sin\gamma \sin\theta) = 0.3^\circ$, which for shoaling ISWs increases the amplitude required for breaking to occur but, from the perspective of nonlinearly steepening bores and hydraulic jumps, allows dispersion time to balance the nonlinearity and form a dispersive wave tail (point 5 above). The observed value of $\gamma_{\mathrm{effective}}$ is furthermore very similar to the angle of 0.52° for which a dispersive wave tail is found to evolve in the numerical results of VH02. It is the influence of the reduced effective

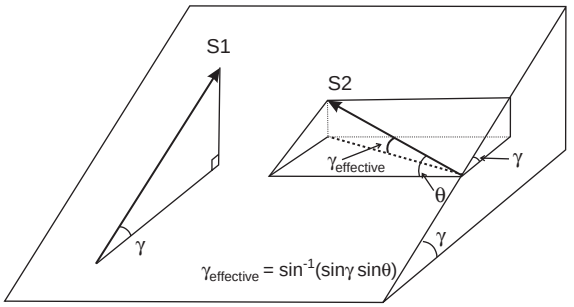

Fig. 16. Schematic indicating the reduced effective slope felt by the solibore during S2 due to an oblique angle of propagation, θ.

slope on the overturning process through the competition between nonlinearity and dispersion that we propose to be the essential difference in the form of S1 and S2.

4.2. Implications for near-bed mixing and sediment resuspension

Transect 1 provided insight into the degree of mixing resulting from an overturning hydraulic jump. Values of $K_z = 10^{-1}\,m^2\,s^{-1}$ are observed at $z = 10\,m$, with more typical values of $10^{-4}\,m^2\,s^{-1}$ sustained throughout the 4 h duration of the solibore. Such a value is of the order of magnitude proposed by Munk and Wunsch (1998) to be required to maintain the thermohaline circulation; however as has been discussed throughout the paper, the solibores occur with a typical period of 4 days and a duration of the order of hours. Thus they are unlikely to contribute significantly to the globally averaged diapycnal mixing. They do, however, have important consequences for mixing in lakes, where wind-forced seiches may occur on a regular basis and degenerate into packets of ISWs (Horn et al., 2001; Boegman et al., 2003) which on reaching the sloping boundary will almost certainly break due to a steeper boundary inclination, γ, as compared to the ocean, thus causing localised mixing as they lose up to 70% of their energy on reflection (Michallet and Ivey, 1999). The results presented here indicate the importance of the obliquity of propagation of ISWs with respect to the slope in determining the effective slope over which they shoal. At oblique angles the effective slope is reduced, potentially resulting in the formation of a dispersive wave train rather than an overturning wave.

The consequences for sediment transport in regions of sloping topography appear to be particularly important. Observations from the FSC suggest that the first solibore, S1, facilitated sediment fluxes $O(10^2)$ larger than the background values, implying that such events completely dominate the mid-slope resuspension (see Bonnin et al. (2002) for the details of the sediment analysis). In contrast to the results of Bogucki et al. (1987), who observe resuspension during periods of low bed-shear stress due to near-bed propagating solitons, we observe resuspension to occur during periods of high bed shear stress in a similar way to Cacchione et al. (2002) who propose that continental slopes are effectively shaped by reflecting internal tides which cause near-bed velocities to generate bed shear stresses high enough to inhibit the deposition of fine-grained sediment. Thomsen and Gust (2000) propose a velocity of $45\,cm\,s^{-1}$ at $z = 1\,m$ is required to resuspend sediment proper, whilst at 700 and 777 m we observe velocities of $>70\,cm\,s^{-1}$ at $z = 8\,m$ during S1. However, the currents at other times during the observational period also exceed $45\,cm\,s^{-1}$ but at which time sediment fluxes were *not* observed to increase, requiring a further explanation beyond the bed shear stress mechanism proposed by Cacchione et al. (2002) as to why fluxes during S1 were so high. We propose that two factors are important in causing the large fluxes; firstly, the rotor formed at the leading edge of the bore will not only bring sediment into suspension due to the strong vertical velocities but will further transport it upwards against the density gradient that otherwise inhibits its vertical transport. This appears to be confirmed at 494 m where, despite comparatively minor enhanced fluxes during S1, the echo intensity from the ADCP provides an indication of suspended matter in the water column. Intensity is largest towards the leading edge where the rotor is observed (Fig. 17A), whilst values are comparatively low during S2 during which no enhanced fluxes were observed (Fig. 17B). A similar mechanism is proposed by Johnson et al. (2001) whereby ISW-induced convergent bottom currents induce vertical motions that lift the nepheloid layer away from the bed in shallow water. Secondly, once brought into suspension, the turbulent boluses are proposed by Helfrich (1992) and Lamb (2002) to be potentially very effective transporters of sediment in an upslope direction. Larger particles are expected to be deposited as the boluses decay whilst finer particles settle out over time and may be advected offshore with the mixed fluid. The results of Bonnin (unpublished results) indicate this to be the case, with the sustained fluxes over day 113 (Fig. 3B) composed of finer particles whilst the flux attributed to the larger particles peaks during the

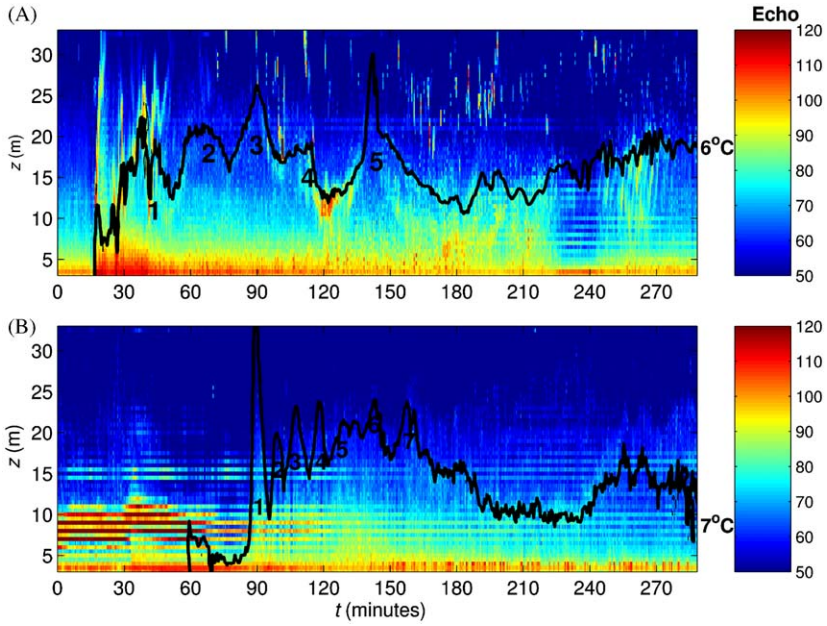

Fig. 17. Echo intensity from ADCP at 494 m during (A) S1 and (B) S2. The mean for each depth bin, $\langle I \rangle$ is removed to account for beam attenuation throughout the water column and values subsequently increased by the minimum value at each depth interval throughout the deployment.

passage of S1 on day 112 and decays immediately following its passage. No enhanced resuspension was observed during S2 when we believe a dispersive wave tail was formed rather than the turbulent boluses. A distinct rotor with comparable vertical velocities was also observed during S2 however, and we propose that the principal reason for the lack of resuspension was the depth at which the solibore originated. The cooler temperature at 471 m depth prior to S2 implies the shallower depression of the thermocline and thus of the point of origin of the solibore as compared to S1; in the FSC available sediment is scoured by the boundary currents at depths of <600 m, with the consequence that there was not any sediment available for resuspension during S2. This further explains why the fluxes during S1 were negligible at 471 m. The long-term (millennial) significance of the up-slope sediment transport has been alluded to by observations of up-slope migrating sedimentary structures in the FSC (Christian Wilson, British Geological Survey, Personal Communication, 2003). High-resolution seismic data indicate a number of agrading mounds over the slope between depths of 500–800 m which are built up on a continuous basis from irregular surfaces, possibly originating from glacial times. Thus the solibore-induced up-slope transport of sediment in the FSC appears to be important to the long-term evolution of the sea-bed topography as well as to the short-term transport of material over the slope.

4.3. Large scale forcing for solibore generation

The results presented here are consistent with the evolution of a hydraulic jump propagating up the slope, due to either shoaling ISWs over a sloping bottom or to the apparently hydraulically supercritical flow prior to the jumps. Given the lack of data from further away from the slope to indicate an incident ISW approaching the slope, we thus consider how a hydraulic jump may be formed at the sea-bed. Specifically, we are concerned with a dynamical mechanism that not only forces perturbations in the thermocline or in the near-bed region over the slope, but does so

with a subinertial periodicity of typically 4 days and is accompanied by current surges in the long-slope direction below the thermocline. Similar 5–6 day periodicities were observed by Thorpe (1987) over the continental slope of the Porcupine Bank which appeared to propagate poleward with a phase speed of 13 cm s^{-1}; thus such signals appear to be commonplace over the north European continental slope.

Internal tides are discounted despite reports by Sherwin (1991) that a deep internal tide exists in the region and is responsible for periodic 'swirls of sand and dust' as reported by the crew of mini-sub operators in the study region. It was considered whether the depression and intensification of the thermocline leading up to S1 brought the slope region at 700 m to criticality for the M_2 semi-diurnal lunar internal tide. The critical frequency is related to the bottom-slope by (Thorpe, 1987)

$$\frac{\sigma^2}{f^2} = \frac{N^2 \sin^2 \gamma}{f^2} + \cos^2 \gamma, \tag{6}$$

where here σ is the frequency of the M_2 tide. Under critical and near-critical conditions, reflecting internal waves may form internal bores which propagate up the slope (Dauxois and Young, 1999), potentially evolving in a similar way to the process of ISW overturning as the stratification is eroded in a band above the bed, bounded at its outer edge by the internal wave characteristic (Legg and Adcroft, 2003). The problem lies in the timing of S1 during a barotropic neap tide when internal tide generation would be expected to be at a minimum. Gerkema (2002) proposes that the strong baroclinic signal at the sea-bed during a barotropic neap tide may be due to a phase shift in the baroclinic spring-neap cycle with respect to the barotropic cycle. Subsequently, enhanced baroclinic signals may be found at the sea-bed but which are intermittent, sensitive to small changes in the background stratification. This is an attractive idea given the variable periodicity of the solibores in the FSC where the background stratification varies, but we discount it because of the concentration in horizontal kinetic energy at a narrow-band subinertial frequency (O(0.3 cycles/days)) observed at depths removed from the bottom by ~100 m during the long-term deployments (Fig. 12). Furthermore, the CTD profiles indicate the slope at 700 m to be subcritical to the M_2 tide (Fig. 18), despite some isolated spikes in the stratification during the second transect which brought small regions of the slope to criticality. The sustained surges in the long-slope current velocity associated with the solibores are also not consistent with semi-diurnal internal tide generation or reflection. One of the principal problems in determining which process may be responsible for the low frequency forcing is the stratification, and in particular its variability in both space and time. Internal wave characteristics are sensitive to changes in the background density field and which will alter the paths taken by the wave; thus any signal at a given point in space and time due to the internal tide may be intermittent on a time scale unrelated to the tide itself but instead due to the different periodicity of variability in the stratification which dictates whether, in the case of the internal tide, the wave is generated and/or reflected or not.

We have considered the possibility that the bottom intensification of currents is due to a bottom-trapped topographic Rossby wave (Rhines, 1970) and which is also dependent on the strength of stratification. Such waves have been proposed to be responsible for a bottom-trapped, 7-day periodicity in the Gulf of Lions (Flexas et al., 2002) and 2–4 and 4–6 day periodicities in the Santa Barbara Channel (Auad et al., 1998). In the FSC, where γ is typically 1°, and $S = N/f \sim 20$, waves become bottom-trapped at frequencies $\sigma < \gamma S$, corresponding to periods >2.5 days and with length scales, $L < 20$ km. The FSC is conducive to type 3 waves in Rhines (1970), requiring $\gamma \ll S^{-1}$ and which have $\sigma \leqslant fS^{-1}$ corresponding to a period of ~10 days. As with the case of internal tides above, the frequency is dependent on the stratification and is thus variable. Thus we do not expect such a motion to occupy a specific frequency in the energy spectra but rather to exhibit a broadband response, again at odds with results from the long-term ADCP. Furthermore, the subinertial currents exhibit little decay away from the bottom, except on day 204, and with no phase propagation (Fig. 13). That the currents at

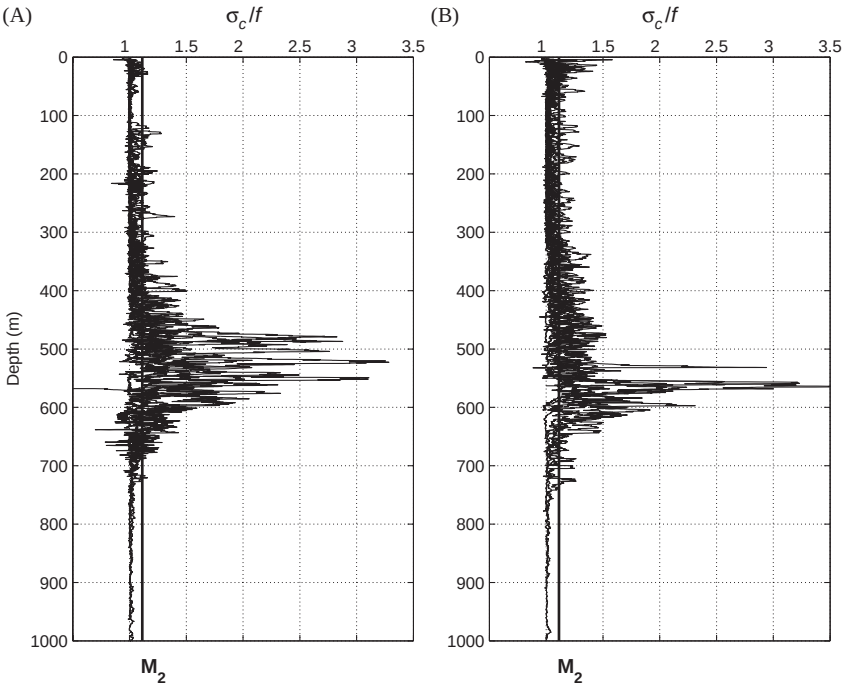

Fig. 18. (A) Critical internal wave frequency, σ_c, normalised over f for CTD profiles conducted during Transect 1 and, (B) Transect 2. Vertical line at $\sigma_c/f = 1.1$ corresponds to the critical frequency for the M_2 internal tide. Profiles are smoothed with a 20 m vertically running mean filter.

605 m are bottom intensified during the passage of the solibores is also subject to debate; the solibores represent the passage of the thermocline up the slope, with the consequence that the flow measured at a particular mooring will be determined by the respective layer within which it is sampling at the time. Thus as the solibore passes a mooring, the instruments will be sampling the lower layer below the thermocline rather than the surface layer prior to the solibore. If the flow in the lower layer is stronger than the upper, the currents measured by an ADCP will appear to be bottom intensified as the lowest bins are in the lower layer, with the signal spreading up as more of the water column is occupied by the fast flowing lower layer.

Thorpe et al. (1995) observe jumps in thermocline depth arising from the interaction of nonlinear internal Kelvin wave fronts with the sloping topography in Lake Geneva which cause a rapid descent of the thermocline and a sudden reversal and intensification of the currents. Along-slope flows may persist for many hours after the wave has passed (Thorpe, 1998). In Section 4.2 it was shown how current pulses prior to S1 and S2 were sufficient to result in hydraulically supercritical conditions, yet in contrast to Holloway (1987) the internal tide is not responsible. We propose that a nonlinear Kelvin wave, propagating to the northeast with the shallow right to the right, may be a potential mechanism facilitating the formation of hydraulic jumps over the sloping bottom, in the same way as proposed by Thorpe (1998). Pressure charts (Fig. 19) indicate that a strong and persistent low-pressure system was situated over the study region from days 110 to112 at which point S1 was observed. As with the observations in Lake Geneva, we expect there to be a lag of approximately 2–3 days, depending on the proximity of the forcing to the study region, between the atmospheric forcing and the oceanic response in the form of the Kelvin wave. Thus it appears that the low pressure system passing to the west of the

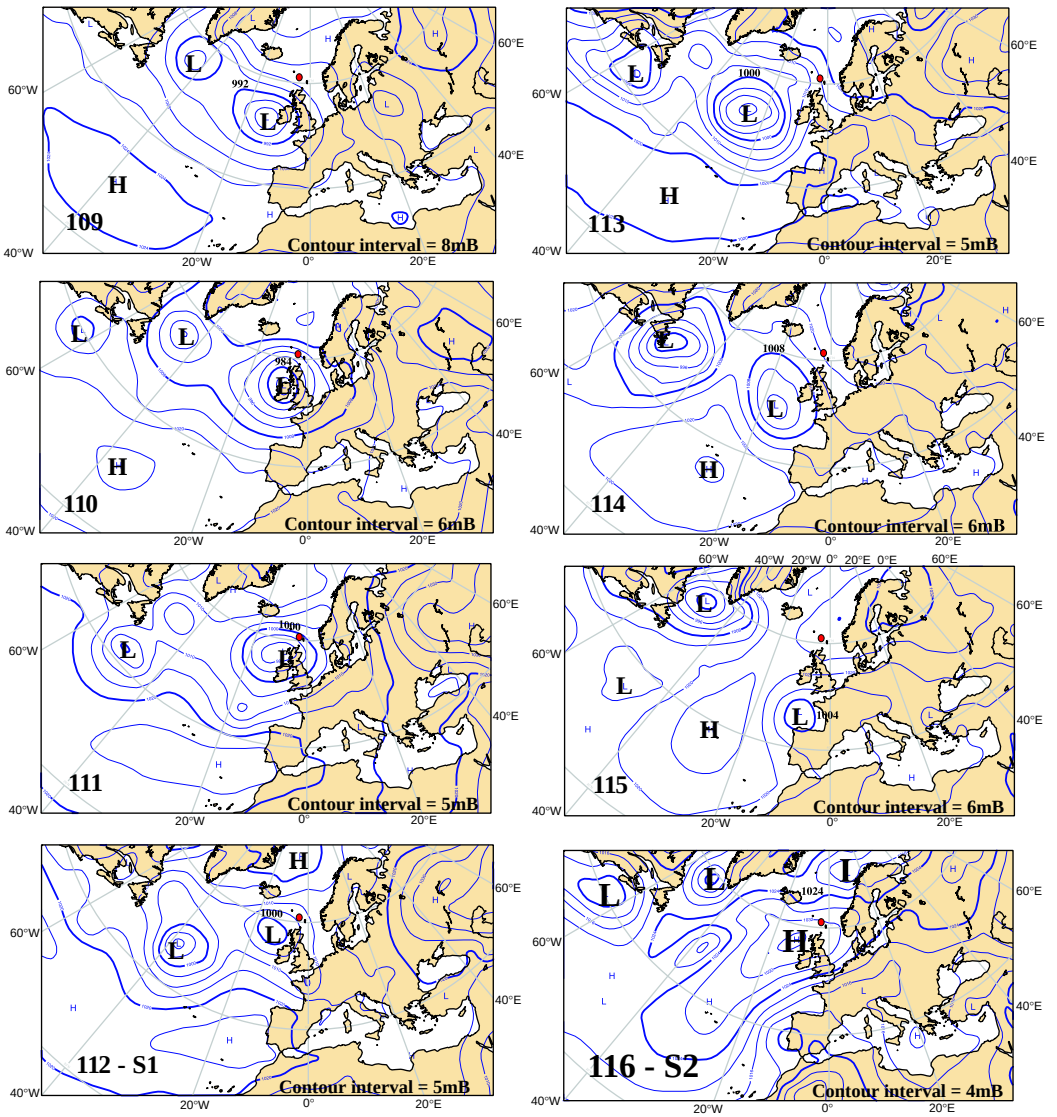

Fig. 19. Mean sea level pressure on days 109–116 (days are indicated in bottom left of each panel), indicating the presence of a persistent low pressure system in the study region prior to S1 up to 112 and a transient low pressure system passing to the west of the study region on days 113 and 114, two days before S2. Low pressure and high pressure are designated by L and H, respectively, and pressure contour intervals are variable; the isobar designated by the thick contour in the study region is labelled and the contour intervals (in mB) are indicated in the bottom right corner of each panel. Approximate position of the moorings are indicated by the red circle. Source: ECMWF ERA-40 Data Set.

study region on days 113 and 114 may be implicated in the forcing of S2. It should be stressed that the different forms of S1 and S2 are due to their response, specifically their angle of propagation with respect to the slope, and not their initial forcing by the Kelvin wave. It is as yet unclear however what factors are important in determining the obliquity of propagation of a solibore resulting from such a process and dedicated future work is needed to elucidate this.

5. Conclusions

During a 12-day measurement period over the continental slope in the FSC, two intense non-linear wave trains were observed propagating up the slope. The wave trains have been described as solibores according to the definition of Henyey and Hoering (1997) with the exception that they do not owe their existence to tidal forcing. They are separated by a period of approximately 4 days and similar signals in the same records and from a long-term deployment suggest a subinertial but variable periodicity to be related to their forcing. We are as yet unable to positively identify the origin of such a periodicity and thus the forcing mechanism of the solibores and propose that the problem lies in an incomplete knowledge of the background stratification to which several of the potential forcing mechanisms are particularly sensitive.

The structure of the solibores is consistent with the results of numerical and laboratory experiments studying overturning hydraulic jumps resulting from shoaling ISWs. Observations of one solibore indicate both the kinematic instability mechanism as being effective and the eventual density and velocity fields to be in accordance with an overturned hydraulic jump. The second solibore propagates at an oblique orientation to the slope however, thereby reducing the effective slope and allowing dispersion to balance the nonlinearity and produce a dispersive wave tail rather than overturning. The density and velocity fields display perturbations with typical solitary wave profiles and particle velocities indicative of genuine solitary waves rather the turbulent boluses resulting from the overturned hydraulic jump. It is shown that hydraulically supercritical conditions were achieved at the sea-bed prior to the solibores, possibly resulting from the passage of a non-linear Kelvin wave, presenting an alternative generation mechanism for the propagating internal hydraulic jump.

The occurrence of such solibores has important implications for understanding the behaviour of internal hydraulic jumps, forced by either shoaling ISWs other sources, propagating over sloping regions in both the oceanic and lacustrine environments. For the latter in particular, ISWs are expected to be significant in the energy transfer from large basin-scale waves to small scales that are available for mixing. In the ocean, the near-bed solibores are very effective at resuspending sediment as shown here by sediment traps deployed near the sea-bed. A rotor, formed by the vertical velocities resulting from the horizontal convergence at the leading edge of the solibore, is proposed to bring sediment into suspension whilst turbulent boluses then transport it up-slope. Support for such a process is provided by seismic data suggesting that the up-slope transport of sediment in the FSC has occurred over a geological timescale and is important in shaping the topography. Given their relative infrequency and short duration, the solibores are not expected to significantly influence the internal wave-induced globally averaged diapycnal diffusivity in the deep-ocean.

Acknowledgments

The data were acquired during the Processes on the Continental Slope (PROCS) project, funded by the Netherlands Organisation for the Advancement of Scientific Research (NWO). We thank the Department of Sea Technology for the preparation of the moorings and the crew of the *RV Pelagia* for their assistance during their deployment and recovery. We are grateful to Jerome Bonnin for the use Figs. 1 and 8 and for his analysis of the sediment traps. We thank Kees Veth for the use of the microstructure data and further thank Theo Hillebrand for his careful and thorough preparation of the instrumentation.

References

Auad, G., Henderschott, M.C., Winant, C.D., 1998. Wind-induced currents and bottom-trapped waves in the Santa Barbara Channel. Journal of Physical Oceanography 28, 85–102.

Boegman, L., Imberger, J., Ivey, G.N., Antenucci, J.P., 2003. High-frequency internal waves in large stratified lakes. Limnology and Oceanography 48 (2), 895–919.

Bogucki, D., Dickey, T., Redekopp, L.G., 1987. Sediment resuspension and mixing by resonantly generated internal

solitary waves. Journal of Physical Oceanography 27, 1181–1196.

Bonnin, J., van Raaphorst, W., Brummer, G-J., van Haren, H., Malschaert, H., 2002. Intense mid-slope resuspension of particulate matter in the Faeroe-Shetland Channel: short-term deployment of near-bottom sediment traps. Deep-Sea Research I 49, 1485–1505.

Bryden, H.L., Candela, J., Kinder, T.H., 1994. Exchange through the strait of Gibraltar. Progress in Oceanography 33, 201–248.

Cacchione, D.A., Pratson, L.F., Ogston, A.S., 2002. The shaping of continental slopes by internal tides. Science 296, 724–727.

Colosi, J.A., Beardsley, R.C., Lynch, J.F., Gawarkiewicz, G., Chjiu, C.-S., Scotti, A., 2001. Observations of nonlinear internal waves on the outer New England continental shelf during the summer Shelfbreak Primer study. Journal of Geophysical Research 106 (C5), 9587–9601.

Dauxois, T., Young, W.R., 1999. Near-critical reflection of internal waves. Journal of Fluid Mechanics 390, 271–295.

Dewey, R.K., Crawford, W.R., Gargett, A.E., Oakey, N.S., 1987. A microstructure instrument for profiling oceanic turbulence in coastal bottom boundary layers. Journal of Atmospheric and Oceanic Technology 4, 288–297.

Djordjevic, V.D., Redekopp, L.G., 1978. The fission and disintegration of internal solitary waves moving over two-dimensional topography. Journal of Physical Oceanography 8, 1016–1024.

Eriksen, C.C., 1982. Observations of internal wave reflection off sloping bottoms. Journal of Geophysical Research 87, 525–538.

Flexas, M.M., Durrieu de Madron, X., Garcia, M.A., Canals, M., Arnau, P., 2002. Flow variability in the Gulf of Lions during the MATER HFF experiment (March–May 1997). Journal of Marine Systems 33–34, 197–214.

Gerkema, T., 2002. Application of an internal-tide generation model to baroclinic spring-neap cycles. Journal of Geophysical Research 107 (C9), 3124.

Grue, J., Jensen, A., Rusas, P.O., Sveen, K.J., 2000. Breaking and broadening of internal solitary waves. Journal of Fluid Mechanics 413, 181–217.

Helfrich, K.R., 1992. Internal solitary wave breaking and run-up on a uniform slope. Journal of Fluid Mechanics 243, 133–154.

Helfrich, K.R., Melville, W.K., Miles, J.W., 1984. On interfacial solitary waves over slowly varying topography. Journal of Fluid Mechanics 149, 305–317.

Henyey, F.S., Hoering, A., 1997. Energetics of borelike internal waves. Journal of Geophysical Research 102 (C2), 3323–3330.

Holloway, P.E., 1987. Internal hydraulic jumps and solitons at the shelf break region on the Australian North West Shelf. Journal of Geophysical Research 92 (C5), 5405–5416.

Horn, D.A., Imberger, J., Ivey, G.N., 2001. The degeneration of large-scale interfacial gravity waves in lakes. Journal of Fluid Mechanics 434, 181–207.

Hosegood, P.J., van Haren, H., 2003. Ekman-induced turbulence over the continental slope in the Faeroe-Shetland Channel as inferred from spikes in current meter observations. Deep-Sea Research I 50 (5), 657–680.

Howell, T.L., Brown, W.S., 1985. Nonlinear internal waves on the California continental shelf. Journal of Geophysical Research 90 (C4), 7256–7264.

Hunkins, K., Fliegel, M., 1973. Internal undular surges in Seneca Lake: a natural occurrence of solitons. Journal of Geophysical Research 78, 539–548.

Jeans, D.R.G., Sherwin, T.J., 2001a. The evolution and energetics of large amplitude nonlinear internal waves on the Portuguese shelf. Journal of Marine Research 59, 327–353.

Jeans, D.R.G., Sherwin, T.J., 2001b. The variability of strongly non-linear solitary internal waves observed during an upwelling season on the Portuguese shelf. Continental Shelf Research 21, 1855–1878.

Johnson, D., Weidemann, A., Scott Pegau, W., 2001. Internal tidal bores and bottom nepheloid layers. Continental Shelf Research 21, 1473–1484.

Kao, T.W., Pan, F.S., Renouard, D., 1985. Internal solitons on the pycnocline: generation, propagation and shoaling and breaking over a slope. Journal of Fluid Mechanics 159, 19–53.

Lamb, K.G., 2002. A numerical investigation of solitary internal waves with trapped cores formed via shoaling. Journal of Fluid Mechanics 451, 109–144.

Legg, S., Adcroft, A., 2003. Internal wave breaking at concave and convex continental slopes. Journal of Physical Oceanography 33 (11), 2224–2246.

Michallet, H., Ivey, G.N., 1999. Experiments on mixing due to internal solitary waves breaking on uniform slopes. Journal of Geophysical Research 104, 13467–13478.

Morozov, E.G., Trulsen, K., Velarde, M.G., Vlasenko, V.I., 2002. Internal tides in the Strait of Gibraltar. Journal of Physical Oceanography 32, 3193–3206.

Munk, W., 1966. Abyssal recipes. Deep-Sea Research 13, 707–730.

Munk, W., Wunsch, C., 1998. Abyssal recipes II: energetics of tidal and wind mixing. Deep-Sea Research I 45, 1977–2010.

New, A.L., Pingree, R.D., 1990. Evidence for internal tidal mixing near the shelf break in the Bay of Biscay. Deep-Sea Research I 37, 1783–1803.

Osborn, T.R., 1980. Estimates of the local rate of vertical diffusion from dissipation measurements. Journal of Physical Oceanography 10, 83–89.

Osborn, AR., Burch, T.L., 1980. Internal solitons in the Andaman Sea. Science 208 (4443), 451–460.

Pingree, R.D., Mardell, G.T., New, A.L., 1986. Propagation of internal tides from the upper slopes of the Bay of Biscay. Nature 321, 154–158.

Rhines, P., 1970. Edge-, bottom-, and Rossby waves in a rotating stratified fluid. Geophysical Fluid Dynamics 1, 273–302.

Sandstrom, H., Elliot, J.A., 1984. Internal tide and solitons on the Scotion Shelf: a nutrient pump at work. Journal of Geophysical Research 89 (C4), 6415–6426.

Sherwin, T.J., 1991. Evidence of a Deep Internal Tide in the Faeroe-Shetland Channel. In: Parker, B.B. (Ed.), Tidal Hydrodynamics. Wiley, New York, pp. 469–488.

Simpson, J.E., 1997. Gravity Currents in the Environment and the Laboratory, Second ed. Cambridge University Press, Cambridge, UK.

Small, J., Sawyer, T.C., Scott, J.C., 1999. The evolution of an internal bore at the Malin shelf break. Annales Geophysicae 17, 547–565.

Smyth, N.F., Holloway, P.E., 1988. Hydraulic jump and undular bore formation on a shelf break. Journal of Physical Oceanography 18, 947–962.

Thomsen, L., Gust, G., 2000. Sediment erosion thresholds and characteristics of resuspended aggregates on the western European continental margin. Deep-Sea Research I 47 (10), 1881–1897.

Thorpe, S.A., 1977. Turbulence and mixing in a Scottish Loch. Philosophical Transactions of the Royal Society of London A 286, 125–181.

Thorpe, S.A., 1987. Current and temperature variability on the continental slope. Philosophical Transactions of the Royal Society of London A 323, 471–517.

Thorpe, S.A., 1998. Some dynamical effects of internal waves and the sloping sides of lakes. In: Imberger, J. (Ed.), Physical Processes in Lakes and Oceans, American Geophysical Union, Coastal and Estuarine Studies, vol. 54, pp. 441–460.

Thorpe, S.A., Keen, J.M., Jiang, R., Lemmin, U., 1995. High frequency internal waves in Lake Geneva. Philosophical Transactions of the Royal Society of London A 354, 237–257.

Turrell, W.R., Slesser, G., Adams, R.D., Payne, R., Gillibrand, P.A., 1999. Decadal variability in the composition of Faroe Shetland Channel bottom water. Deep-Sea Research I 46, 1–25.

van Haren, H., Groenewegen, R., Laan, M., Koster, B., 2001. A fast and accurate thermistor string. Journal of Atmospheric and Oceanic Technology 18, 256–265.

Vlasenko, V., Hutter, K., 2002. Numerical experiments on the breaking of solitary internal waves over a slope-shelf topography. Journal of Physical Oceanography 32, 1779–1793.

Wallace, B.C., Wilkinson, D.L., 1988. Run-up of internal waves on a gentle slope in a two-layered system. Journal of Fluid Mechanics 191, 419–442.

Wesson, J.C., Gregg, M.C., 1988. Turbulent dissipation in the strait of Gibraltar and associated mixing. In: Nihoul, J.C.J., Jamart, B.M. (Eds.), Small-Scale Turbulence and Mixing in the Ocean. Elsevier, Amsterdam, pp. 201–212.